



THE UNIVERSITY *of* EDINBURGH

Edinburgh Research Explorer

AhR controls redox homeostasis and shapes the tumor microenvironment in BRCA1-associated breast cancer

Citation for published version:

Kubil, S, Bassi, C, Roux, C, Wakeham, A, Göbl, C, Zhou, W, Jafari, SM, Snow, B, Jones, L, Palomero, L, Thu, KL, Cassetta, L, Soong, D, Berger, T, Ramachandran, P, Baniasadi, SP, Duncan, G, Lindzen, M, Yarden, Y, Herranz, C, Lazaro, C, Chu, MF, Haight, J, Tinto, P, Silvester, J, Cescon, DW, Petit, A, Pettersson, S, Pollard, JW, Mak, TW, Pujana, MA, Cappello, P & Gorrini, C 2019, 'AhR controls redox homeostasis and shapes the tumor microenvironment in BRCA1-associated breast cancer', *Proceedings of the National Academy of Sciences (PNAS)*, vol. 116, no. 9, pp. 3604-3613.
<https://doi.org/10.1073/pnas.1815126116>

Digital Object Identifier (DOI):

[10.1073/pnas.1815126116](https://doi.org/10.1073/pnas.1815126116)

Link:

[Link to publication record in Edinburgh Research Explorer](#)

Document Version:

Peer reviewed version

Published In:

Proceedings of the National Academy of Sciences (PNAS)

General rights

Copyright for the publications made accessible via the Edinburgh Research Explorer is retained by the author(s) and / or other copyright owners and it is a condition of accessing these publications that users recognise and abide by the legal requirements associated with these rights.

Take down policy

The University of Edinburgh has made every reasonable effort to ensure that Edinburgh Research Explorer content complies with UK legislation. If you believe that the public display of this file breaches copyright please contact openaccess@ed.ac.uk providing details, and we will remove access to the work immediately and investigate your claim.



AhR controls redox homeostasis and shapes the tumour microenvironment in BRCA1-associated breast cancer

Shawn Kubli¹, Bassi Christian¹, Cecilia Roux¹, Andrew Wakeham¹, Christoph Göbl¹, Wenjing Zhou¹, Bryan Snow¹, Lisa Jones¹, Luis Palomero², Kelsie Thu¹, Luca Cassetta³, Daniel Soong³, Thorsten Berger¹, Parameswaran Ramachandran¹, Shakiba Baniyasadi⁴, Gordon Duncan¹, Moshit Lindzen⁵, Yosef Yarden⁵, Carmen Herranz², Conxi Lazaro², Mandy Fang-chi¹, Jillian Haight¹, Paul Tinto¹, Jennifer Silvester⁶, David Cescon⁷, Anna Petit¹, Sven Pettersson⁸, Jeffrey Pollard⁹, Tak W. Mak⁴, Miguel Pujana², Paola Cappello¹⁰, Chiara Gorrini¹

¹Princess Margaret Hospital, ²Institut d'Investigació Biomèdica de Bellvitge, ³University of Edinburgh, ⁴The Campbell Family Institute for Breast Cancer Research at Princess Margaret Cancer Centre, University Health Network, ⁵The Weizmann Institute, ⁶Campbell Family Institute for Breast Cancer Research at Princess Margaret Cancer Centre, University Health Network, ⁷The Campbell Family Institute for Breast Cancer Research at Princess Margaret Cancer Centre, Ontario Cancer Institute, Princess Margaret Cancer Centre/University Health Network, ⁸Nanyang Technological University, Singapore, ⁹College of Medicine and Veterinary Medicine, ¹⁰Turin University

Submitted to Proceedings of the National Academy of Sciences of the United States of America

Cancer cells have higher reactive oxygen species (ROS) than normal cells due to genetic and metabolic alterations. An emerging scenario is that cancer cells increase ROS to activate pro-tumorigenic signaling while activating antioxidant pathways to maintain redox homeostasis. Here we show that, in Basal-like and BRCA1-related breast cancer (BC), ROS levels correlate with the expression and activity of the transcription factor, Aryl hydrocarbon Receptor (AhR). Mechanistically, ROS triggers AhR nuclear accumulation and activation to promote the transcription of both antioxidant enzymes and the epidermal growth factor receptor (EGFR) ligand, amphiregulin (AREG). In a mouse model of BRCA1-related BC, cancer-associated AhR and AREG control tumor growth and production of chemokines to attract monocytes and activate pro-angiogenic function of macrophages in the tumor microenvironment. Interestingly, the expression of these chemokines as well as infiltration of monocyte-lineage cells (monocyte and macrophages) positively correlated with ROS levels in Basal-like BC. These data support the existence of a coordinated link between cancer-intrinsic ROS regulation and the features of tumor microenvironment. Therapeutically, chemical inhibition of AhR activity sensitizes human BC models to Erlotinib, a selective EGFR tyrosine kinase inhibitor, suggesting a promising combinatorial anti-cancer effect of AhR and EGFR pathway inhibition. Thus, AhR represents an attractive target to inhibit redox homeostasis and modulate the tumor promoting microenvironment of Basal-like and BRCA1-associated BC.

triple negative breast cancer | aryl hydrocarbon receptor | reactive oxygen species | tumor-associated macrophages | amphiregulin

INTRODUCTION

Cancer cells have a highly dynamic and heterogeneous metabolism that enable them to generate energy, maintain redox homeostasis and undertake biosynthesis (1, 2). In addition, cancer metabolism has the ability to influence the communication of the tumor cells with nearby immune cells by controlling the nutrient status of the surrounding tumor microenvironment (TME)(3-6). Hence, the study of cancer-associated metabolic alterations has presented attractive therapeutic opportunities in several pre-clinical models of cancers, including breast, colorectal and lung cancer (7-9).

Among all forms of breast cancer (BC), the Basal-like (commonly being triple-negative based on defined markers; TNBC) is generally more aggressive, of poor prognosis and frequently appears in women carriers of mutations in the tumor suppressor BRCA1. More and more evidence supports the idea that the study of TNBC dysregulated metabolism will lead to efficacious therapeutic approaches against this aggressive disease (10). Compared to other BC subtypes, these cancers have increased glutamine consumption and heightened sensitivity to glutamine

depletion(11). Moreover, in addition to BRCA1 mutations, this subtype harbors loss-of-function mutations in Tp53 tumor suppressor which together promote antioxidant responses(12, 13). Therefore, Basal-like BC tends to accumulate higher levels of reactive oxygen species because of its genetic and metabolic alterations.

Here we found that human BC with low expression or inactivation of BRCA1 specifically express aryl hydrocarbon receptor (AhR), a ligand-activated transcription factor that regulates the expression of a large superfamily of antioxidant molecules known as cytochrome p450 proteins (CYP1A1, CYP1A2, and CYP1B1) (14). In normal and malignant mammary cells, AhR activity is triggered by ROS induced by glutathione deprivation or absence of functional NRF2 antioxidant function. In the same conditions, AhR directly promotes the expression of amphiregulin (AREG), a ligand of the epidermal growth factor receptor (EGFR).

Using *in vitro* and *in vivo* models of basal-like/TNBC, we demonstrate that AhR-AREG signaling pathway positively supports tumorigenesis by controlling ROS and shaping the pro-tumorigenic functions of TME. Furthermore, chemical- and genetically-induced AhR loss-of-function sensitizes tumor cells

Significance

Basal-like/BRCA1-associated breast cancer (BC) is a very aggressive form of BC that frequently occurs in young women with devastating effects. Since tailored therapies are lacking for this type of tumor, scientists and clinicians are searching for weaknesses that can be therapeutically exploited. Here we describe the role of the transcription factor, Aryl hydrocarbon Receptor (AhR), in supporting BC growth by controlling ROS levels and the tumor-promoting features of the microenvironment. In BC cells, AhR activation mediates the link between intracellular ROS regulation and the pro-tumorigenic functions of the surrounding immune system. We propose that tailored inhibition of AhR-regulated pathways can lead to BC eradication by pushing it beyond its ROS tolerance limit and deprive it of tumor-supporting immune cells.

Reserved for Publication Footnotes

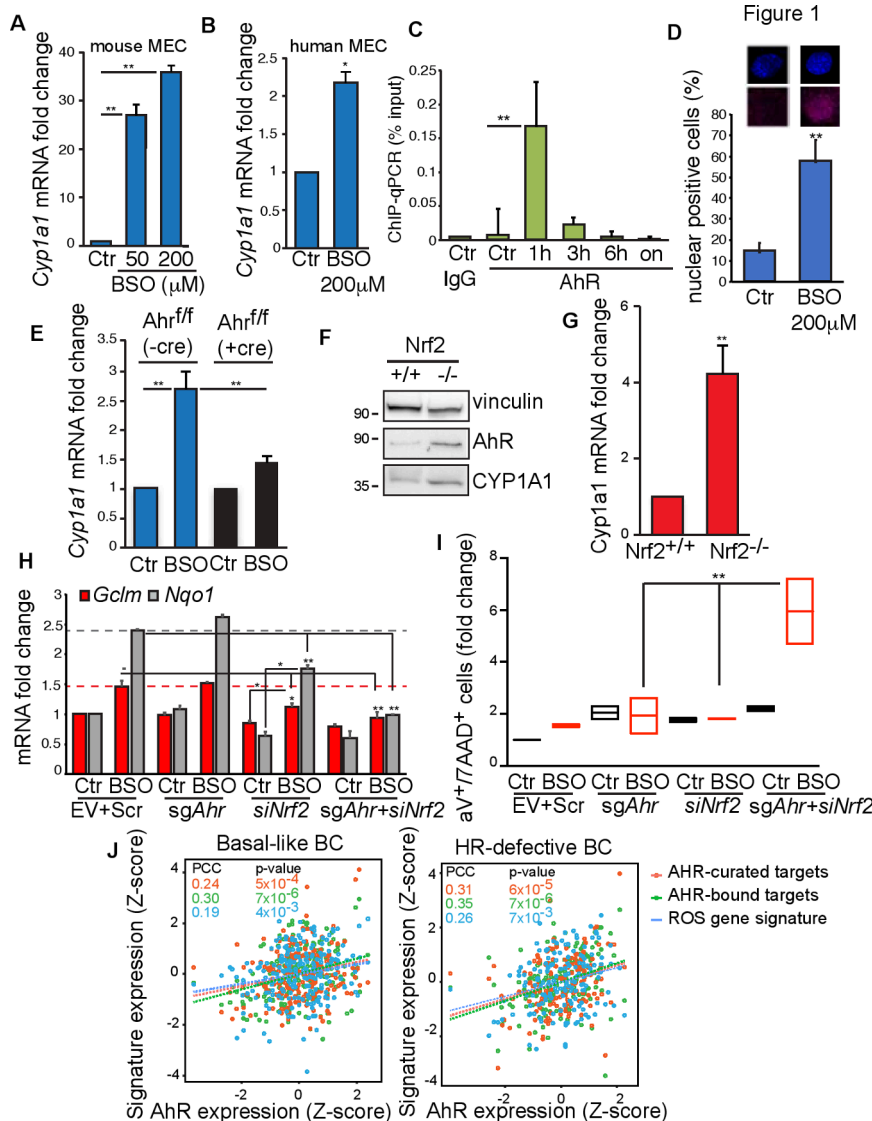


Figure 1
Fig. 1. AhR is activated by ROS in normal and malignant mammary epithelial cells. (A) *Cyp1a1* mRNA levels in mouse MEC left untreated (Ctr) or treated with 50 μM and 200 μM BSO for 24hr. (B) *CYP1A1* mRNA levels in human MCF10A cells treated left untreated (Ctr) or treated 200 μM BSO for 24h. (C) ChIP-qPCR assay to detect AhR on *Cyp1a1* promoter in COMMA-1D cells treated with 200 μM BSO for indicated time points (n=3/group). ChIP with IgG antibody was used as a negative control. (D) Representative images of immunocytochemistry analysis of AhR nuclear staining in cells treated with BSO (200 μM for 2h) or left untreated (Ctr). Bar graph shows the percentage of nuclear AhR positive cells (n=100). Additional examples are reported in SI Appendix, Figure S1B. (E) *Cyp1a1* mRNA levels in MEC that were isolated from *Ahr*^{fl/fl} mice, infected with Cre-expressing (+cre) or empty vector control (-cre) adenoviruses, and then treated or not with 50 μM BSO for 24hr (n=3/group). (F) Immunoblot showing AhR and CYP1A1 proteins in *Nrf2*^{+/+} or *Nrf2*^{-/-} MEC. Vinculin, loading control. (G) *Cyp1a1* mRNA levels in MEC isolated from *Nrf2*^{+/+} or *Nrf2*^{-/-} female mice (n=5/genotype). (H) mRNA analysis of NRF2-targets *Gclm* and *Nqo1* in COMMA-1D cells that were transfected with single guide RNA against mouse *Ahr* (*sgAhR*) and then subjected to BSO (200 μM) for 24h. Cells manipulated with empty vector (EV) and non-targeting (scramble, scr) siRNA were used as control. n=3/group. (I) COMMA-1D cells were treated as in (H), harvested 48h post-treatment and stained with annexinV/7-AAD apoptosis detection kit. (J) Positive association between AhR expression, AHR-curated targets, AHR-bound targets and the "ROS gene signature" in basal-like and Homologous Recombination (HR) Defective BC within the TCGA human BC dataset. See Material and Methods for details. PCC=Pearson's Correlation Coefficient.

to erlotinib, an EGFR inhibitor, thus suggesting a promising combinatorial anti-tumor strategy for the treatment of TNBC.

RESULTS

AhR is activated by ROS in normal and malignant mammary cells

AhR redox activity has been mainly associated with the detoxification of xenobiotics and pollutants (15), while NRF2 with the regulation of glutathione metabolism (2). However, studies of AhR or NRF2 knockout mice suggest a potential crosstalk between these factors in the maintenance of redox homeostasis (16). We found that long-term treatment of mouse and human mammary epithelial cells (MEC) with buthionine sulfoximine (BSO), a glutathione synthesis inhibitor (17) led to increased expression of AhR antioxidant target *Cyp1a1* but did not affect *Ahr* mRNA levels (Fig. 1A, B and SI Appendix, Fig. S1A). This was due to the ability of AhR to bind the *Cyp1a1* promoter as shown by chromatin immunoprecipitation (ChIP) assay followed by qPCR in cells treated with BSO at different time points (Fig. 1C). Compared to IgG antibody control, AhR recruitment peaked at 1h post-treatment, suggesting that BSO can trigger AhR transcriptional activity as rapidly as the well-characterized AhR ligand,

2,3,7,8-tetrachlorodibenzo-p-dioxin (TCDD)(18, 19). Immunocytochemistry assay showed a high frequency of cells positive for nuclear AhR after 2h exposure to BSO when compared to control conditions (Fig. 1D and SI Appendix, Fig. S1B). To further test the specificity of AhR activation of *Cyp1a1* by BSO, we isolated primary MEC from the mammary glands of female *Ahr* conditional knock-in mice (*Ahr*^{fl/fl}) in which Cre recombinase excises exon.2 encoding the basic domain responsible for DNA-binding (20). As expected, *Ahr* exon.2 expression was found to be relatively lower in *Ahr*^{fl/fl} MEC infected with Cre-expressing adenovirus (SI Appendix Fig. S1C). In these settings, BSO-induced upregulation of *Cyp1a1* was significantly abrogated (Fig. 1D).

The evidence that AhR could respond to the intracellular depletion of reduced glutathione prompted us to test the relationship between AhR and NRF2 in the control of ROS levels in normal and malignant MEC. Compared to MEC isolated from *Nrf2* wild-type (*Nrf2*^{+/+}) female mice, MEC from *Nrf2* null (*Nrf2*^{-/-}) mice did not express *Nrf2* mRNA and accumulated both AhR and *Cyp1a1* proteins (Fig. 1E and SI appendix Fig. S1D). These changes were associated with an increase in *Cyp1a1* mRNA while AhR levels were not affected (Fig. 1F and SI Appendix Fig. S1E). NRF2 bona fide target *Hmox1* was downregulated while *Nqo1*

Figure 2

Figure 3

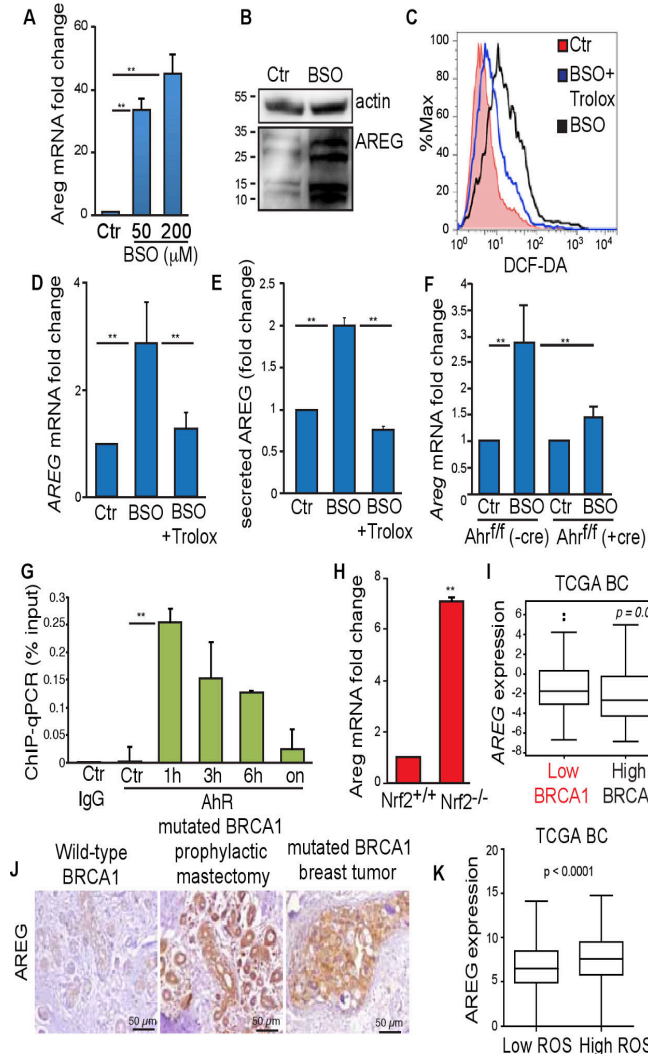


Fig. 2. AREG expression is regulated by ROS-activated AhR and is elevated in BRCA1-associated BC. (A) *Areg* mRNA levels in mouse MEC that were left untreated (Ctr) or treated with the indicated doses of BSO for 24hr (n=3/group). (B) Immunoblot showing AREG protein in mouse MEC that were left untreated (Ctr) or treated with 200μM BSO for 24hr. Vinculin, loading control. (C) Representative FACS profile of ROS levels in mouse cells treated with 200μM BSO, with or without 250μM Trolox and stained with DCF-DA after 24h. (D) *Areg* mRNA in mouse cells treated as in (C) (n= 3/group). (E) ELISA measurement of secreted AREG protein in culture medium of mouse cells treated as in (C) (n=5/group). (F) *Areg* mRNA levels in MEC that were isolated from *Ahr*^{fl/fl} mice, infected with Cre-expressing (+cre) or empty vector control (-cre) adenoviruses, and treated or not with 50μM BSO for 24hr (n=3/group). (G) ChIP-qPCR assay to detect AhR on *Areg* promoter in COMMA-1D cells treated with 200μM BSO and harvested at the indicated time points (n=3/group). ChIP with IgG antibody was used as a negative control. (H) *Areg* mRNA in MEC isolated from *Nrf2*^{+/+} or *Nrf2*^{-/-} virgin female mice (n=5/genotype). (I) *AREG* mRNA levels in TCGA BC grouped according to low (bottom tertile) or high (top tertile) BRCA1 expression (n=1102). (J) Representative images of IHC to detect AREG protein in samples from a BRCA1 wild-type reduction mammoplasty from healthy women used as controls, a prophylactic mastectomy in a woman heterozygous for a BRCA1 mutation (BRCA1 mutant), and a human BRCA1 mutant basal/TNBC breast tumor. (K) Expression levels of AREG in Basal-like BC with "low ROS" or "high ROS" based on the "ROS gene signature".

mRNA was unaffected in *Nrf2*^{-/-} as compared to *Nrf2*^{+/+} cells (SI Appendix Fig. S1F,G). Then, the consequences of downregulated *Ahr* and/or *Nrf2*, (separately or in combination) were assessed.

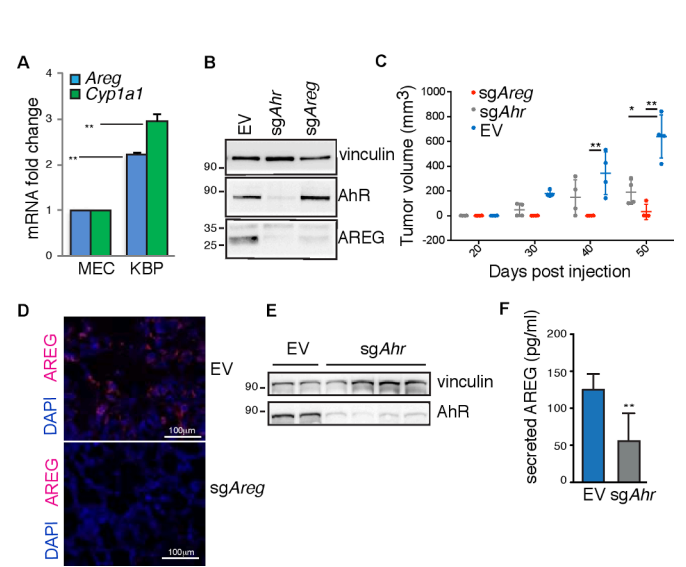
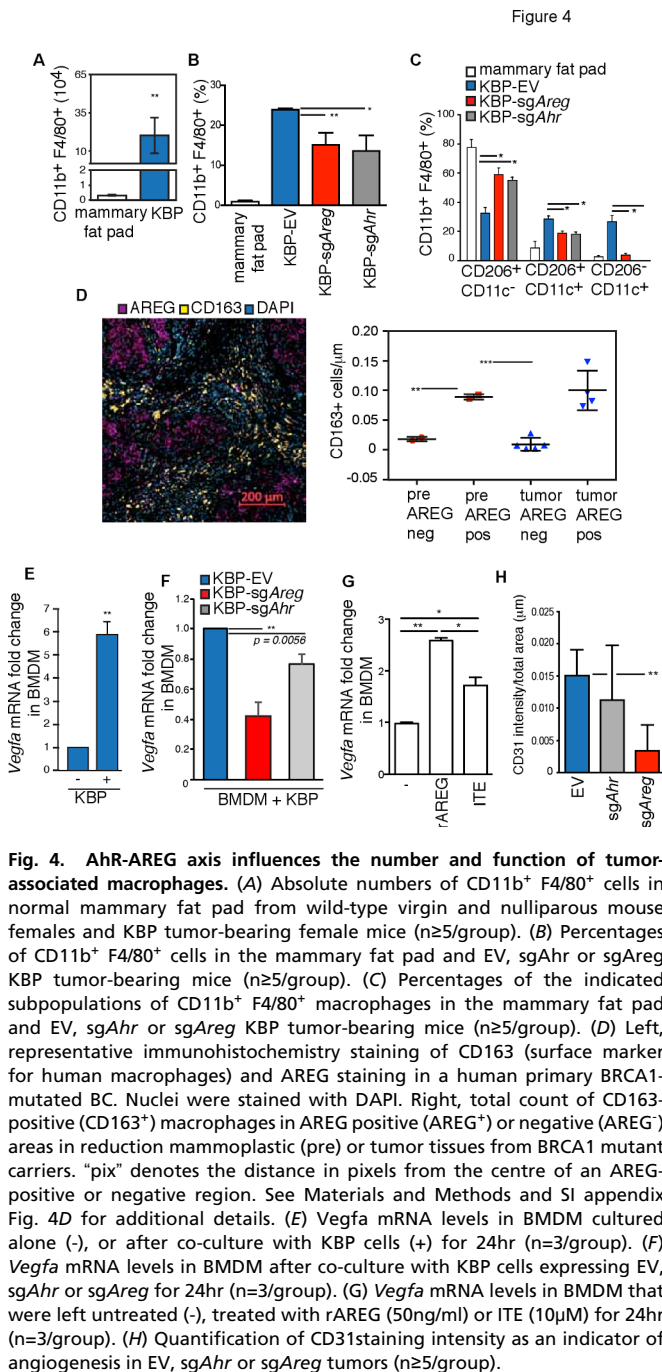


Fig. 3. AhR and AREG support tumorigenesis in a mouse model of BRCA1-associated BC. (A) Levels of *Areg* and *Cyp1a1* mRNAs in mouse MEC and KBP cells (n=3/group). (B) Immunoblot showing AhR and AREG proteins in lysates from KBP tumors transfected with empty vector (EV) and single guide RNAs against mouse *Ahr* (sgAhr) or *Areg* (sgAreg) and selected in puromycin-containing media for three days. Vinculin, loading control. (C) Representative plot of tumor volume increase over time in FVB female mice transplanted with KBP cells expressing EV, sgAhr or sgAreg (n=4/group). (D) Representative immunofluorescence staining of nuclei (DAPI) and AREG protein (red) in EV and sgAreg KBP tumors. (E) Immunoblot showing AhR protein in lysates from EV and sgAhr KBP tumors. Vinculin, loading control. (F) ELISA measurement of AREG protein in lysates from EV and sgAhr KBP tumors.

Briefly, first we deleted *Ahr* by cell transfection with single guide RNA (sgAhr) followed by puromycin selection, then we applied *Nrf2* siRNA (siNrf2) for one day prior BSO treatment. Control cells (Ctr) were left untreated and additional controls were generated for *Ahr* and *Nrf2* downregulation by applying an empty sgRNA vector (EV) and a non-targeting (scramble, Scr) siRNA, respectively. Cells were collected at 24h and 48h for RNA and apoptosis analysis, respectively. *Nrf2* mRNA levels were low in siNrf2-transfected cells, as compared to Scr control (SI Appendix Fig. S1H). *Cyp1a1* expression was specifically affected by sgAhr in both untreated (Ctr) and BSO-treated cells (SI Appendix Fig. S1I). In EV+Scr cells, NRF2 targets *Nqo1* and *Gclm* were properly upregulated by BSO treatment within 24h, while they were not affected in sgAhr samples and marginally altered in siNrf2 cells. Low levels of both *Ahr* and *Nrf2* dramatically decreased BSO-induced *Nqo1* and *Gclm* levels (Fig. 1G). This resulted in a significant increase in apoptosis in *Ahr/Nrf2*-deleted cells as measured by annexinV/7-AAD staining (Fig. 1H).

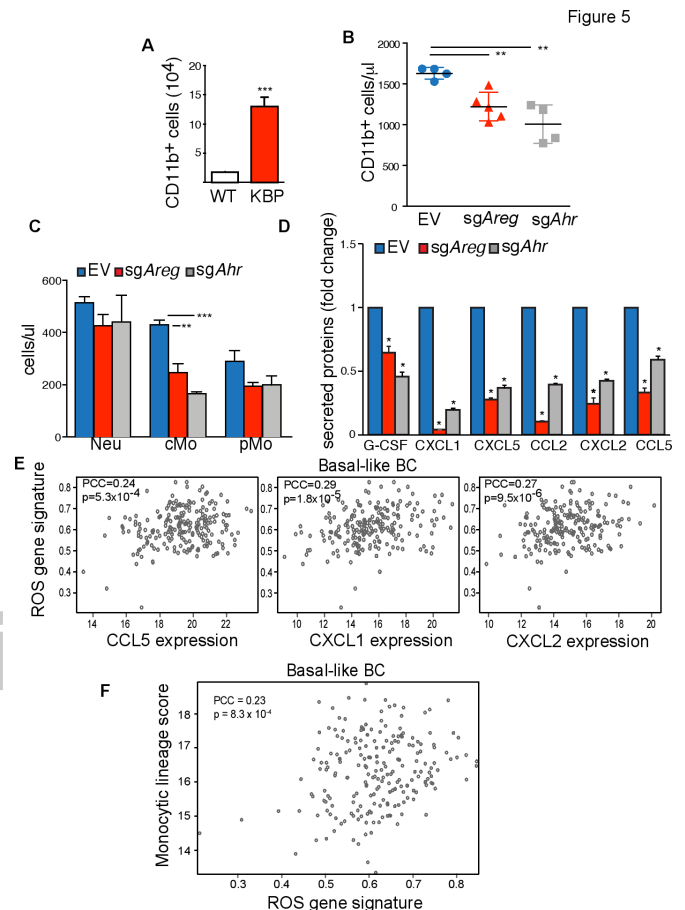
We next examined whether AhR activation could also be a marker of oxidative stress in human basal-like/TNBC. The expression of AhR and its canonical targets, *CYP1A1* and *CYP1B1*, were found to be higher in BC with genetic mutations (Van't Veer dataset) or low expression (TCGA cohort) of BRCA1 gene (SI Appendix Fig. S1J,K). Through bioinformatics analysis of TCGA data of basal-like BC and BC with homologous recombination DNA repair defects (HR-defective BC, see Methods for additional details), we found that expression of *Ahr* gene and two *Ahr*-regulated gene sets positively correlated with an oxidative stress gene expression signature (Fig. 1I)(21). Together, these data indicate that both NRF2 and AhR may act as sensors of oxidative stress in normal and malignant MEC.-



ROS-regulated AhR controls expression of the epidermal growth factor receptor ligand, amphiregulin

Cells use non-toxic levels of ROS to activate specific signaling pathways that regulate proliferation and malignant transformation (22). Furthermore, some studies have reported a correlation between xenobiotic-induced AhR activation and high levels of the epidermal growth factor receptor (EGFR) ligand, amphiregulin (AREG)(23, 24). Therefore, we tested the hypothesis that AhR could modulate the EGFR pathway in conditions of oxidative stress in addition to an antioxidant response. In primary mouse MEC and in non-tumorigenic human breast epithelial cells (MCF10A), BSO greatly induced AREG protein levels (Fig. 24,B and SI Appendix Fig. S24).

EGFR is a member of a large family of receptor tyrosine kinases that also includes HER2 (ERBB2/NEU), ERBB3, and



ERBB4. All these receptors promote intracellular signaling in the form of homo- or heterodimers and upon binding to a large spectrum of soluble ligands including EGF, epiregulin (EREG), amphiregulin (AREG), epigen (EPGN), neuregulin (NRG1/2/3/4), transforming growth factor alpha (TGFalpha) and Heparin-binding EGF-like growth factor (HB-EGF) (25). In different cancer types, Erbb receptors and ligands are differentially regulated during tumorigenesis and influence tumor progression and response to therapies(26, 27).

To verify the specificity of Areg regulation by ROS in MEC, we assessed the expression of different Erbb ligands in mouse MEC treated with BSO. Of note, these cells mainly express *Egfr*, *Erbb2* and *Erbb3* receptors (SI Appendix Fig. S2B). In these cells, among all known Erbb ligands, BSO mainly induced the expression of Areg (SI Appendix Fig. S2C). Areg mRNA upregulation by BSO appears to be ROS-mediated, since co-treatment of human MEC with the antioxidant Trolox abolished both BSO-induced ROS and the accumulation of this transcript (Fig. 2C,D). Once translated, AREG is a membrane-bound protein whose

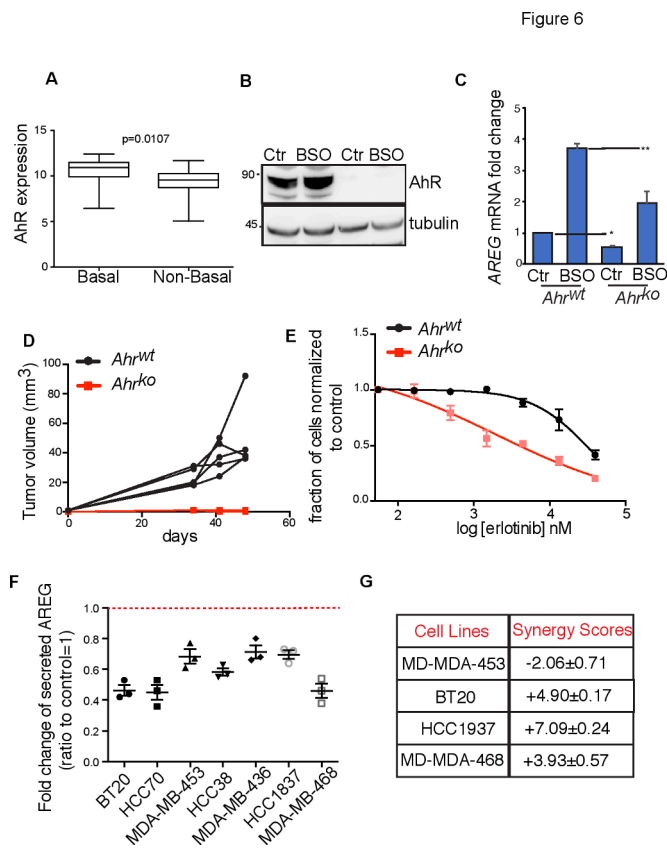


Fig. 6. AhR-AREG axis is a promising therapeutic target in basal-like and BRCA1-associated BC. (A) AhR expression levels in basal-like versus non-basal-like BC cell lines included in the Cancer Cell Line Encyclopedia. See Material and Methods for details. (B) Immunoblot of MDA-MB-468 cell line carrying a wild-type (*Ahr^{wt}*) or deleted form of AhR (*Ahr^{ko}*). Cells were left untreated (Ctr) or exposed to 500μM BSO for 24h. (C) AREG mRNA levels in cells treated as in (B). (D) Representative plot of tumor volume increase over time after transplantation of MDA-MB-468 *Ahr^{wt}* and *Ahr^{ko}* cells in the fat pad of immune-compromised NOD-SCID female mice. (E) Sensitivity of MDA-MB-468 *Ahr^{wt}* and *Ahr^{ko}* cells to increasing doses of EGFR inhibitor, Erlotinib, as measure by SRB growth assay. (F) Levels of secreted AREG in the media of the indicated cell lines after treatment with the AhR inhibitor (CH-223191) for 24h and represented as ratio to their respective AREG levels in control (untreated) conditions. n=3. (G) Synergy scores for the AhR inhibitor, CH-223191 (AhRi) and Erlotinib in the indicated BC cell lines as calculated using the SynergyFinder web application (see Material and Methods for details and SI Appendix Fig. S7).

activation is regulated by release of its extracellular domain from the membrane (28). Indeed, BSO treatment promoted AREG release into the culture medium of MCF10A cells in a Trolox-sensitive manner (Fig. 2E).

Next, we investigated whether AhR was involved in regulating AREG expression. MEC isolated from female *Ahr^{fl/fl}* mice were infected with Cre-expressing adenovirus prior exposure to BSO. Thus, BSO-induced upregulation of *Areg* was abrogated by loss of transcriptional activity of AhR (Fig. 2F). This suggested that, like *Cyp1a1* (Fig. 1D), *Areg* might be a direct AhR transcriptional target. Indeed, a putative XRE element (5'-G/T N T/G GCGTG A/C-3') was identified at -260bp from the ATG start codon. COMMA-1D cells were treated with BSO for different time points prior to ChIP-qPCR assay. Compared to IgG antibody control, AhR enrichment at *Areg* promoter started at 1h post-treatment and gradually declined overtime (Fig. 2G).

Figure 7

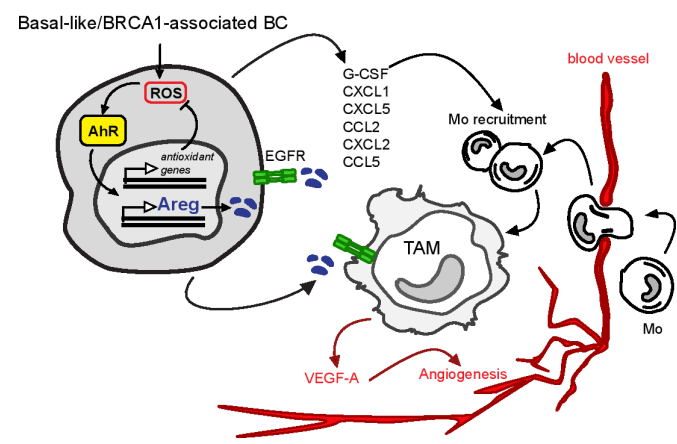


Fig. 7. AhR-AREG axis defines a novel signaling pathway between cellular intrinsic redox mechanisms and surrounding TME. See Discussion for detailed description.

It is worth noting that MEC from *Nrf2^{-/-}* mice accumulated more Areg mRNA than MEC from *Nrf2^{+/+}* mice, ruling out that the transcript increase is regulated by NRF2 (Fig. 2H).

In the TCGA dataset, AREG expression was also found to be higher in BC with low levels of BRCA1 (Fig. 2I). Moreover, by immunohistochemistry assay (IHC), AREG protein expression was found to be significantly elevated in mammary pre-neoplastic tissues of BRCA1 mutation carriers and in the corresponding advanced tumors (Fig. 2J and SI Appendix S2D). Consistently, in the TCGA BC dataset, AREG levels were also associated with a high ROS score (Fig. S2K). Therefore, AREG is a novel transcriptional target of AhR in MEC and its expression correlates with AhR and ROS levels in human BC.

AhR-AREG axis is required for BRCA1-associated mammary tumorigenesis

To characterize the functional involvement of the AhR-Areg axis in basal-like and BRCA1-associated tumors, we took advantage of a transplantable mouse primary mammary tumor cell line (KBP) isolated from a mammary tumor arising in the K14cre *Bracl^{fl/fl} Trp53^{fl/fl}* basal-like/TNBC mouse model (29). Mammary tumors originating from KBP cells resemble spontaneous basal-like/TNBC (30). Compared to normal MEC, the NRF2 target *Nqo1* was previously shown to be downregulated in mouse and human Basal-like/TNBC tumors, as a consequence of defective NRF2 function (12). However, *Nqo1* was still induced by exposure to BSO in these cells, suggesting a coordinated transcriptional control of this gene by NRF2 and AhR as shown in Fig. 1 (SI Appendix S3A). AhR targets *Cyp1a1* and *Areg* were highly expressed in KBP cells, as compared to normal MEC (Fig. 3A). We then used CRISPR/Cas9 gene editing to delete mouse *Ahr* and *Areg* in mammary tumor cells by transient transfection. KBP cells with single guide (sg) RNA against *Ahr* (*sgAhr*) or *Areg* (*sgAreg*) were maintained under selection for three days prior to analysis *in vitro* or transplantation *in vivo*. The *sgAreg* and *sgAhr* treatments of KBP cells did not affect their proliferation prior transplantation (SI Appendix Fig. S3B) but did induce a significant decrease in AREG and AhR proteins as compared to cells transfected with control empty vector (EV) (Fig. 3B). Notably, *Ahr* deletion also reduced AREG protein, confirming that Areg is an AhR downstream target (Fig. 3B).

Next, we transplanted EV-, *sgAreg*- or *sgAhr*-transfected KBP cells into the mammary fat pads of virgin female mice

and monitored tumor growth until EV-treated tumors reached humane endpoint (tumor volume=1cm³). Tumor development in mice receiving either sgAreg- or sgAhr-transfected KBP cells was significantly reduced compared to animals receiving EV-KBP cells (Fig. 3C and SI Appendix Fig. S3C). *Areg* deletion almost completely prevented the expansion of KBP tumor cells in vivo, possibly as a result of a cell-autonomous requirement for AREG in these cells. Indeed, *Areg* deletion in KBP cells impaired cell growth in vitro as shown by Sulforhodamine B (SRB) assay over a period of 12 days (SI Appendix Fig. S3D).

We confirmed that small tumors growing from sgAreg-treated cells showed a significant reduction in AREG expression measured by IHC (Fig. 3D). sgAhr-treated cells had almost undetectable expression of AhR that consequently affected AREG secretion (Fig. 3E,F). Then, we tested if AREG was the main Erbb ligand to be regulated by AhR in KBP tumors. RNA sequencing (RNA-seq) showed a similar expression profile of Erbb receptors but higher levels of *Areg*, *Hbegf* and *Nrg1* ligands were observed in KBP tumors as compared to normal mammary gland tissue (SI Appendix Fig. S3E). However, neither *Hbegf* nor *Nrg1* expression levels were affected by *Ahr* deletion as compared to *Areg*, further underlying the existence of a specific AhR-AREG axis in these tumors (SI Appendix Fig. S3F).

AhR-AREG axis regulates the phenotype and function of macrophages in BRCA1-deleted mouse mammary tumors

AhR and AREG are both expressed in innate and adaptive immune cell populations to regulate immunity, inflammation and tissue repair (31, 32). However, apart from a few studies (33-35), the roles of these proteins in the TME is still uncertain. Macrophages are the most abundant immune cells recruited to the breast tumor site, where they become "tumor-associated macrophages" (TAM). TAM have complex genetic and molecular characteristics resulting in extraordinary plasticity and are particularly abundant in BC and present at all stages of progression (36). To examine the characteristics of TAM, we first analyzed macrophages resident in normal mammary tissue of virgin and nulliparous FVB female mice. These cells typically expressed integrin α M chain (CD11b), EGF-like module-containing mucin-like hormone receptor-like 1 (F4/80), MER proto-oncogene tyrosine kinase (MerTK) and cluster of differentiation 64 (CD64) (37), as well as the mannose receptor C type 1 (MRC1/CD206) (SI Appendix Fig. S4A), which is also expressed by TAM (SI Appendix Fig. S5B) (38). KBP tumors showed a significant increase in CD11b⁺F4/80⁺ macrophages as compared to mammary fat pad (Fig. 4A). These macrophages expressed EGFR phosphorylation at tyrosine 106, suggesting activation of EGFR in TAM as previously found in another tumor models (39, 40) (SI Appendix Fig. S4C). Compared to control tumors, KBP tumors from sgAreg- or sgAhr-treated cells had less CD11b⁺F4/80⁺ macrophages with a surface marker profile of non-tumorigenic, tissue-resident macrophage in the mammary fat pad (Fig. 4B,C).

Next, the relevance of TAM in *BRCA1*-deficient human BC was quantified. IHC staining for CD163 showed that tumor-associated AREG expression correlated with high density and close proximity of macrophages in both pre-neoplastic (reduction mammary) and tumors from *BRCA1* mutant carriers, (Fig. 4D and SI Appendix Fig. S4D). Collectively, these data postulate a role of AhR-AREG signaling in attracting TAM into the breast TME.

One well described function of TAM is to produce vascular endothelial growth factor-A (VEGF-A), which facilitates angiogenesis and metastasis (41). In vitro co-culture systems between KBP cells and bone-marrow derived macrophages (BMDM) showed that BMDM had a dramatic increase in *Vegfa* mRNA expression after being in contact with tumor cells (Fig. 4E). These changes contributed to an overall increase in the level of secreted VEGF-A protein in the culture medium of KBP-BMDM co-

cultures (SI Appendix Fig. S4E). In contrast to BMDM, KBP cells maintained a high basal level of *Vegfa* mRNA that did not change after co-culture (SI Appendix Fig. S4F). VEGF-A production by BMDM was mainly AREG dependent since deletion of KBP-associated *Areg* strongly reduced *Vegfa* expression in BMDM in co-culture systems (Fig. 4F). Furthermore, recombinant AREG (rAREG) significantly increased *Vegfa* mRNA levels in BMDM to a higher extent than ITE-mediated AhR activation (Fig. 4G). We also discovered a significant increase in EGFR expression in BMDM after co-culture with KBP cells, further supporting the ability of BMDM to respond to AREG-mediated signaling (SI Appendix Fig. S4G). Collectively, these data support the ability of cancer-associated AhR and AREG expression to affect the density and tumor-supporting properties of TAM within mammary TME. Corroborating these in vitro findings, we found that sgAreg tumors had less CD31-positive endothelial cells, indicating a low degree of tumor vasculature (Fig. 4H).

AhR-AREG axis influences myeloid cell recruitment in BRCA1-deleted mouse mammary tumors

Normal mammary ductal genesis is characterized by the epithelial cell-dependent recruitment of monocytes, which mature in situ into macrophage that provide critical support for developing tissue (42). Similarly, during mouse BC tumorigenesis monocytes can be recruited by developing mammary tumors, where they mature into pro-tumoral TAM characterized by high CD11c expression (43). Furthermore, increases in peripheral blood monocytes is a key feature of human and mouse malignancies, which correlates positively with TAM density in human cancer (44). We found that KBP tumor-bearing animals contained increased numbers of CD11b⁺ monocytes in the peripheral blood (Fig. 5A). In contrast, monocytes were significantly reduced in the peripheral blood of sgAreg and sgAhr tumor bearing mice (Fig. 5B). Further stratification of these cells revealed significantly reduced numbers of classical monocytes (cMo; CD11b⁺Ly6-C^{hi}Ly6-G⁻CX3CR1⁺) in the blood of sgAreg and sgAhr tumor mice, with no significant changes in neutrophils (CD11b⁺Ly6-C^{int}Ly6-G⁺CX3CR1⁺) or patrolling monocytes (pMo; CD11b⁺Ly6-C^{int/lo}Ly6-G⁻CX3CR1⁺) (Fig. 5C).

The recruitment and activation of monocytes and macrophages are regulated by specific chemokines and cytokines in the TME (45). Compared to MEC, KBP cells released significantly higher levels of chemokines important for the recruitment and activation of monocytes and macrophages such as granulocyte-colony stimulating factor (G-CSF), chemokine (C-X-C motif) ligand 1 (CXCL1), C-X-C motif ligand 5 (CXCL5), C-C motif chemokine ligand 2 (CCL2), C-X-C motif ligand 2 (CXCL2) and C-C motif chemokine ligand 2 (CCL5) (SI Appendix Fig. S5A) (46). Interestingly, sgAreg and sgAhr KBP tumor cells displayed significantly lower production of all chemokines elevated in KBP control cells (Fig. 5D). Treatment of sgAhr tumor cells with recombinant AREG (rAREG) considerably rescued the levels of G-CSF, CXCL1, CXCL5, CCL2, CXCL2 and CCL5 chemokines (SI Appendix Fig. S6B). This result suggests that AhR expression affects chemokine production through AREG modulation. Mouse data were validated by analysis of human BC in the TCGA cohort. Expression of *CXCL1*, *CXCL2* and *CCL5* chemokines correlated positively with *Ahr* and *AREG* expression and was high in BC with low *BRCA1* levels (SI Appendix Fig. S5C). Interestingly, these chemokines were also increased in basal-like BC with high ROS content (Fig. 5E), along with an elevated infiltration of monocytic lineage cells (monocytes and macrophages) in the TME (Fig. 5F). Our data show that AhR-AREG pathway stimulates the recruitment of monocytic cells in the TME and these changes correlate with high levels of cancer-associated ROS in basal-like BC.

AhR-AREG axis is a promising therapeutic target for human BRCA1-associated BC

Then, we sought to test the oncogenic role of AhR in human BC as previously performed in the mouse model. As found in TCGA data analysis, *AhR* mRNA expression was more elevated in basal-like versus non-basal-like BC cell lines (Fig. 6A). Next, we a

MDA-MB-468 cells were CRISPR/Cas9 edited to obtain stable isogenic cell lines that were proficient (*AhR* wild-type, *AhR*^{wt}) or deficient for AhR (*AhR* knock-out, *AhR*^{ko}). Compared to *AhR*^{wt}, *AhR*^{ko} cells did not express AhR and consequently they had a significant low level of AREG and CYP1A1 expression at both basal level and upon exposure to BSO (Fig. 6B,C and SI Appendix Fig. S6A). In these cells, *AhR* deletion dramatically impaired their ability to both grow in vitro and form tumor in the mammary fat pad of immunodeficient NOD-scid female mice (Fig. 6D and SI Appendix Fig. S6B). Given the low levels of *Areg* mRNA in *AhR*^{ko} cells, we tested their sensitivity to Erlotinib, an EGFR tyrosine kinase inhibitor (47). AREG expression has been associated with resistance to EGFR inhibitors in breast, lung and colon cancers(48-51). Compared to *AhR*^{wt} tumor cells, *AhR*^{ko} cells were highly sensitive to EGFR inhibition as measured by a standard 5-day SRB assay (Fig. 6E).

The above results prompted us to evaluate the therapeutic value of interfering with AhR oncogenic function through the use of a potent and specific AhR inhibitor (AhRi), namely CH-223191(52). Treatment of a subset of basal-like BC cell lines with 1μM CH-223191 for 24h significantly reduced secretion of AREG, independently of the variability of AREG basal level in these cells (Fig. 6F and SI Appendix Fig. S6C). In both MDA-MB-468 and HCC1937, treatment with AhR inhibitor affected AREG secretion in a dose-dependent manner and in the absence of any external stimulus (SI Appendix Fig. S6D,E). Consistent with this finding, CH-223191-treated HCC-1937 cells showed a defect in the EGFR phosphorylation normally induced by incubation in nutrient-rich culture medium as compared to untreated cells or cells exposed to Erlotinib, an EGFR tyrosine kinase inhibitor⁵⁵ (SI Appendix Fig. S6F). These data suggest that AhR inhibition by a chemical compound can affect EGFR activation.

Given the effect of AhR inhibition on AREG levels and EGFR phosphorylation, we investigated whether the targeting of AhR might synergize with Erlotinib treatment to curtail BC cell growth. We seeded MDA-MB-453, BT20, MDA-MB-468 and HCC1937 cells in 96-well plates and treated them with various combinations of Erlotinib and CH-223191. Erlotinib was used at 3-fold serial dilution starting at 25μM (5 dilutions total) while CH-223191 was used at 3-fold serial dilution starting at 50μM (9 dilutions total). First, we scored drug toxicity by calculating cell density using the sulforhodamine B (SRB) colorimetric assay. Then, we determined if there was any synergy in therapeutic activity between CH-223191 and Erlotinib using SynergyFinder⁵⁶. This analysis revealed a high degree of therapeutic synergy between Erlotinib and CH-223191 in cell lines with high EGFR expression (BT20, MDA-MB-468 and HCC1937), but an antagonistic effect where EGFR expression was low (MDA-MB-453) (Fig. 6G and SI Appendix Fig. S7). These findings demonstrate a therapeutic potential of targeting both the cell-extrinsic (secreted AREG) and cell-intrinsic (intracellular AhR activation) components of the AhR-AREG axis for the treatment of BRCA1-associated BC.

DISCUSSION

To date, most of the studies focused on AhR are linked to its role as environmental sensor for dioxins and xenobiotics. Recent work has elucidated a multitasking role of AhR in the control of cancer cell survival and tumor-associated immune system functions(53). The fact that AhR is chronically activated in many tumor types, including BC, supports the premise that AhR might

be a promising drug target for anti-cancer therapies. However, the benefits of targeting AhR is still under debate given the contradictory observations that AhR is both pro-tumorigenic and a tumor suppressor and the multitude of activities elicited by different AhR ligands (14). In our work, analysis of human BC data and the use of human and mouse BC models supports an oncogenic role of AhR in Basal-like and BRCA1-associated BC. In addition to controlling ROS, AhR stimulates transcription of the EGFR ligand AREG and thereby activates EGFR signaling in both normal and malignant MEC. Interestingly, among all known ErbB ligands, AREG is the main target of ROS-activated AhR pathway. Thus, AhR ensures cell survival and proliferation by coordinating an antioxidant response and activating the potent tumor-promoting signaling pathway mediated by EGFR. Indeed, AhR deletion by CRISPR/Cas9 gene editing dramatically impaired the in vivo growth of mouse and human TNBC cells.

Besides controlling cell intrinsic functions, AhR signaling influences the infiltration and phenotypic properties of macrophages in the TME. Tumor-infiltrating macrophages take on a trophic role that facilitates angiogenesis, extracellular matrix breakdown, and tumor cell motility, particularly in BC (41). Conversely, human BC cells can educate macrophages to adopt a tumorigenic and immunosuppressive phenotype that allows the BC cells to avoid immune surveillance and continue their invasion and growth (54). In our tumor model, we have found that AhR and its downstream effector AREG regulate a cluster of monocyte/macrophage-related chemokines that shape the immune landscape of BRCA1-deficient mammary tumors, resulting in an increase in CD11b+F4/80+CD206+ TAM with a tumorigenic phenotype. Indeed, our co-culture of mouse BRCA1-deficient tumor cells with BMDM provides a clear demonstration of the mutual communication between macrophages and tumor cells in the expression of VEGF-A and the control of tumor angiogenesis. Analysis of TCGA human BC dataset have corroborated the correlation between myeloid-related chemokines (CCL5 and CXCL1/2) and expression levels of BRCA1, AhR and AREG. Strikingly, the expression of these chemokines and the presence of myeloid populations is associated with Basal-like BC with high ROS content.

Overall, our observations suggest the following model (graphically summarized in Fig. 7). In basal-like/TNBC or BRCA1-associated BC, genetic and metabolic alterations may lead to chronic high ROS levels that trigger an increase in AhR protein levels and transcriptional activity. In these conditions, AhR activation counters ROS by promoting expression of antioxidant genes but it also induces the expression of EGFR ligand, AREG. Through the release of AREG and specific chemokines (G-CSF, CXCL1/2/5 and CCL2/5) in the TME, AhR activation axis may facilitate the recruitment of monocytes from blood vessels and the activation of pro-tumorigenic and angiogenic TAM.

In conclusion, we have established a novel connection between tumor-intrinsic redox mechanisms and TME composition in BC. Our in vivo work using a *Brcal1/Trp53*-deleted mouse model reveals how both these aspects are prerequisites for tumor progression and maintenance. These observations provide valuable insights into the multifactorial oncogenic activity of AhR and may form the basis of a better tailored future drug development against one of the most aggressive and challenging type of BC.

Materials and Methods

Mice

K14cre BRCA1^{fl/fl} p53^{fl/fl} (KBP) mice were provided by Dr. J. Jonkers (NKI, Amsterdam, The Netherlands) and were on the FVB background. KBP tumor cells were obtained and used for in vivo transplantation studies as described(30). NRF2^{-/-} mice were kindly provided by Dr. P. Ohashi (Princess Margaret Cancer Centre, Toronto, Canada) and were on the C57/B6 background. AhR^{fl/fl} mice were purchased from The Jackson Laboratory (stock no: 006203) and were on a mixed background. For mouse and human tumor transplantation studies, FVB and immune-deficient NOD-SCID recipient

female mice were 8-10 week old and were purchased from The Jackson Laboratory. All mice were maintained and handled according to protocols approved by the Animal Care and Use Committee of the University Health Network (UHN; Toronto, Canada).

Cell lines and treatments

Mouse COMMA-1D cells (originally provided by S. Muthuswamy, Ontario Cancer Institute, Toronto, Canada), primary mouse MEC, and KBP cells were cultured in DMEM/F12 medium containing 10% FBS (Thermo Fisher Scientific), L-glutamine, 1 μ g/ml hydrocortisone (Sigma), 5 μ g/ml insulin (Sigma), and 5 ng/ml epidermal growth factor (EGF, Sigma). Human MCF10A cells (ATCC) were cultured in DMEM/F12 medium supplemented with 5% horse serum (Thermo Fisher Scientific), 20 ng/ml epidermal growth factor (EGF), 0.5 μ g/ml hydrocortisone, 100 ng/ml cholera toxin (Sigma), 10 μ g/ml insulin, and penicillin-streptomycin (Pen-Strep, Thermo Fisher Scientific). Human breast cancer cell lines (ATCC) were cultured under strain-specific conditions according to ATCC recommendations.

Oxidative stress was induced for various times by exposing cells to medium containing 50 μ M or 200 μ M buthionine sulfoximine (BSO, Sigma). For ROS scavenging, BSO-exposed cells were co-treated with 250 μ M Trolox (EMD Millipore). MEC were starved in 0.5% FBS and nutrient-free medium for 24h and then treated in the same medium with 50ng/ml recombinant AREG from R&D Systems (262-AR-100) and harvested after 24 hr. The AhR antagonist CH-223191 (Sigma) was applied to cell cultures at 1 μ M, 5 μ M and 10 μ M for 24h (AREG measurement by ELISA), 900nM (analysis of EGF receptor phosphorylation in HCC1937) or different doses for 5 days (drug screening). The tyrosine kinase inhibitor, Erlotinib, was administered to HCC1937 cell line at 600nM for analysis of EGF receptor phosphorylation by Western Blot.

Isolation of primary murine mammary epithelial cells (MEC)

Primary murine MEC were isolated from 8-10 week old virgin female mice as previously described(12). MEC were cultured in serum-free medium for 48 hr to kill stromal fibroblasts and seeded (5x10⁵) in 6-well plates for experiments. In the case of AhR^{fl} mice, MEC (1x10⁵) were seeded in 6-well plates and infected overnight with pre-packaged, ready-to-use adenovirus expressing Cre recombinase (Vector BioLabs, PA, USA). Cells were processed for analysis 48 hr after infection.

Preparation of murine bone marrow-derived macrophages (BMDM)

Whole bone marrow was harvested from 10-12 week old female mice by flushing Hanks' Balanced Salt Solution (HBSS) through femurs and tibias using a 27-gauge needle (BD Biosciences). Following red blood cell lysis, cells were cultured in 10% RPMI in 10cm plates overnight. Non-adherent cells were collected and reseeded in petri dishes in medium containing 20 ng/ml murine macrophage colony-stimulating factor (M-CSF; Peprotech). After 3 days of culture, cells were provided with fresh medium containing 20ng/ml M-CSF. Macrophages were harvested on day 4.

For co-culture experiments, BMDM (1x10⁶) were seeded in triplicate in 6-well plates and incubated with or without KBP cells (2.5x10⁵ cells/well). Cells were harvested 48 hr later using enzyme-free cell dissociation medium (Millipore) and either processed for flow cytometric analysis or sorted as described in Flow Cytometry and Sorting.

Mouse and human tumor induction and treatment

KBP (3x10⁵) or MDA-MB-468 (0.5x10⁶) cells were transplanted into #4 mammary gland fat pads of syngeneic FVB or NOD-SCID female mice (10 weeks old). Diameters of developing tumors were measured in duplicate using digital calipers starting on day 14 (KBP) or day 30 (MDA-MB-468) post-transplantation when tumors became palpable. Tumor volume (mm³) was calculated as $\frac{1}{2}(\text{width}^2 \times \text{height})$. Tumor diameters were measured and volumes calculated as above two times per week.

Mouse mammary tumor dissociation for FACS analysis

Tumors were resected from #4 mammary fat pads of transplanted mice, cut into 2-3mm² pieces, and placed into a C-tube (Miltenyi Biotech) containing 5 ml Iscove's Modified Dulbecco's Medium (IMDM) supplemented with 10% FBS, 2 mM L-glutamine, 100 U/ml penicillin, 100 μ g/ml streptomycin, 0.05 mM β -mercaptoethanol, 0.26 U/ml Liberase TM (Sigma), and 20 U/ml DNase I (Sigma). Tumors were mechanically processed using a gentleMACS Octo Dissociator with Heaters (Miltenyi Biotech). Processed samples were filtered once through a 100 μ m cell strainer (Falcon), and the corresponding C-tubes were rinsed with 5 ml cold IMDM and passed through the same strainer. Cells were filtered once using a 70 μ m strainer (Falcon), followed by a 40 μ m strainer (Falcon). Filtered samples were collected in 15 ml Falcon tubes and centrifuged at 1250 RPM for 8 min at 4°C. Pellets were incubated with red blood cell lysis buffer for 7 min at room temperature (RT), and then centrifuged at 1250 RPM for 8 min at 4°C before resuspension in PBS-/- containing 1% bovine serum albumin (BSA) plus 2 mM ethylenediaminetetraacetic acid (EDTA). Cell suspensions were subjected to fluorescence-activated cell sorting (FACS)/flow cytometry as described below.

Flow cytometry and cell sorting

Flow cytometric analyses of tumor-associated macrophages (TAM) and BMDM were performed using the following Abs: anti-CD49f-AF488 GoH3, anti-CD45.1-AF700 A20, anti-CD11b-Pacific Blue M1/70, anti-F4/80-PE BM8, anti-CD206-APC C068C2, anti-CD11c-APCCy7 N418, and anti-MHCII-PECy7 M5/114.15.2 (all from BioLegend). For FACS experiments, macrophages were identified as CD49f^{lo}-CD45⁺CD11b⁺F4/80^{hi} and sorted to >95% purity into 10% RPMI at 4-8°C. BMDM were further processed for RNA extraction (see

below), while TAM were seeded into 96-well flat-bottom plates at 2x10⁵ cells/well. For flow cytometric analysis of resident macrophages in mammary glands of naive FVB mice, the additional Abs anti-MerTk-PE 108928 (R&D Systems) and anti-CD64-PE X54-5/7.1 (BioLegend) were applied.

For analysis of peripheral blood monocytes, blood (15 μ l) was collected from the tail veins of live mice into a heparinized capillary tube, followed by transfer into a 5 ml polystyrene tube containing 100 μ l PBS-/- plus 20 mM EDTA. Peripheral blood samples were stained directly with anti-Ly6C-PE HK1.4, anti-Ly6G-APCCy7 1A8, and anti-F4/80-FITC BM8 (BioLegend) Abs in combination with the Abs described above.

All flow cytometry samples were blocked for a minimum of 10 min in 1:100 anti-CD16/CD32 2.4G2 (eBioscience) containing 1:200 DNase I (protease-free, Roche) prior to staining in PBS-/- containing 1% BSA plus 2 mM EDTA. After blocking, Abs were added at appropriate dilutions and cells were stained for 30 min on ice. Dead cells were excluded by adding 5 μ l 7-AAD (BioLegend) during the last 10 min of surface staining. Cells were then washed and either sorted on an Astrios FACS Instrument (Beckman Coulter), or analyzed using a Fortessa Instrument (BD Bioscience) and FlowJo software (Tree Star, Inc.).

For flow analysis of phosphorylated EGFR, tumors were dissociated according to mouse mammary tumor dissociation method. 10⁶ cells were suspended in 0.5 ml PBS-/- and fixed with 0.5 ml of 4% formaldehyde (final concentration 2%) for 10 min at 37°C. Cells were washed by centrifugation with PBS-/- containing 1% BSA and 2 mM EDTA prior staining with anti-CD49f (AF488 GoH3; 1/200), anti-CD45.1 (AF700 A20; 1/400), anti-CD11b (Pacific Blue M1/70; 1/400) and anti-F4/80-PE (BM8; 1/400) for 30min on ice. Cells were then washed twice and permeabilized by adding ice-cold Perm Buffer II (BD) with gently vortexing. Cells were incubated for 30 min on ice and washed twice. Cells were then suspended in 100 μ l of primary phospho-EGF Receptor (Tyr1068) antibody (D7A5, 1:1600, Cell signaling) and incubated for 1h on ice. Cells were washed twice and then resuspended in 100 μ l of secondary antibody (goat anti-rabbit APC conjugated, ThermoFisher Scientific, 1/1000) and incubated for 1h on ice. Cells were washed twice and analyzed at Fortessa Instrument (BD Bioscience) and data were processed with FlowJo software (Tree Star, Inc.).

CRISPR/Cas9 gene-editing

For CRISPR/CAS9 gene-editing studies in mouse and human cells, single guide RNAs were evaluated using two different online CRISPR design tools: the MIT online CRISPR Design Tool (<http://crispr.mit.edu/>), and the Zinc Finger Consortium Tool (<http://zifit.partners.org/Zifit/CSquare9Nuclease.aspx>). To minimize potential off-target mutations, we selected highly specific guide RNA sequences which were predicted to have zero potential off-targets; even after 3 mismatches in the 20 nucleotide sgRNA sequence. The following oligos were used to synthesize mouse guide target sequences: mouse AhR, forward primer 5'-CACCGTAGCGTACGTACCTGA-3' and reverse primer 5'-AAACRCAGGTAGCTGACGCTGAGC-3'; and mouse Amphiregulin, forward primer 5'-CACCGGTGGACTTGAGCTTCTGT-3' and reverse primer 5'-AAACA-CAGAAAGCTCAAGTCCACC-3'. For CRISPR/CAS9 gene-editing of human AhR in MDA-MB-468, an sgRNA targeting human AhR exon1 (NC.000007.14) was designed. The following guide oligos were designed to express the sgRNA: forward primer 5'-CACCGTCACCTACGCCAGTCGCAAG-3' and reverse primer 5'-AAACCTTGGAGTGGCGTAGGTGAC-3'. In all cases, the annealed double-stranded guide oligo was cloned into the BbsI cut puromycin-modified version of vector pX330 (Addgene plasmid # 42230). To obtain a stable MDA-MB-468 line carrying AhR deletion, the pX330-PURO hAhR-sgRNA plasmid vector was transfected into cells using Lipofectamine 3000 (ThermoFisher), followed by brief selection pressure in 1 μ g/ml puromycin for 48 hours, and isolation of resistant individual clonal cell lines after 2 weeks. A 748 bp genomic PCR amplicon spanning the human AhR exon1 CRISPR/CAS9 sgRNA target sequence was amplified using the forward primer: 5'-CACGCCACTGTCCGAGAGGACGACGAGGTG-3', and reverse primer: 5'-TATGAGC-GCAACACAAAGCCAGTTGGTGG-3'. Direct DNA sequencing of the human AhR exon1-spanning genomic DNA PCR amplicon was performed using the sequencing primers: forward 5'-AGTGGTCCGACCTACAC-3' and reverse 5'-GCTGTCAACAAATCAGGACC-3'. Human AhR exon1 CRISPR/CAS9 frame-shift modifications on each allele was verified by analysis of DNA sequence chromatograms. Human and mouse AhR knock-out was further verified and validated using RT-PCR of downstream targets or Western blotting with AhR specific antibody (BML-SA210-0025, Enzo Life Sciences).

siRNA and sgRNA cell transfection

COMMA-1D, KBP and MDA-MB-468 cells (1x10⁵) were seeded into 6-well plates and transfected overnight with specific plasmids plus Lipofectamine 3000 (Life Technologies). For studies of AhR and NRF2 combinatorial downregulation, COMMA-1D cells were first transfected with empty vector or empty vector containing AhR single guide RNA, then kept in medium with 1 μ g/ml puromycin (Wisent Bio Products) for 2 days prior transfection with mouse NRF2 siRNA (50pmo, Thermo Fisher Scientific). KBP transfected cells were cultured in medium with 1 μ g/ml puromycin for 72 hr prior to injection into #4 mammary fat pads of syngeneic female FVB mice. MDA-MB-468 cells were cultured and maintained in medium containing 1 μ g/ml puromycin until expansion of stable resistant clones.

Cell proliferation measurement

1089 KBP cells expressing empty vector and sgRNA against mouse Areg and
 1090 AhR were analyzed for proliferation by using 488 EdU Click Proliferation Kit
 1091 (BD Biosciences), accordingly to manufacture's guidelines.

1092 **Apoptosis measurement**

1093 Apoptosis was evaluated by Annexin V/7-AAD staining. In brief, cells
 1094 were collected and stained with FITC-conjugated Annexin V and 7-AAD for 15
 1095 min at room temperature in 10 \times binding buffer. All reagents were purchased
 1096 from BD Biosciences. Cells were analyzed by a FACSCalibur flow cytometer
 immediately after staining.

1097 **Cell growth measurement**

1098 KBP cells were transfected with sgAhr, sgAreg or EV as described above.
 1099 Positive selection was applied using 1 μ g/ml puromycin for 48 hours. Cells
 1100 were then resuspended, counted and plated in 6-well plates. Cells were
 1101 fixed at the indicated time points for subsequent SRB assay analysis. Time
 1102 points were seeded in triplicate. Cell number was assessed indirectly by
 using the Sulforhodamine B (SRB) colorimetric assay (Sigma) according to
 the manufacturer's recommendations.

1103 **Drug sensitivity screening**

1104 Human breast cancer cell lines were seeded at different concentrations
 1105 accordingly to the cell line to obtain 30% confluency in 96-well plates in
 1106 triplicate. After 24 hr, cells were treated with Erlotinib at 3-fold serial dilution
 1107 starting at 25 μ M (5 dilutions total) and/or CH-223191 at 3-fold serial dilution
 1108 starting at 50 μ M (9 dilutions total). Cells were maintained in culture for 5
 1109 days before calculating cell density using the sulforhodamine B (SRB) colori-
 1110 metric assay (Sigma) according to the manufacturer's recommendations. Cell
 density was calculated using the SoftMax Pro software (Molecular Devices).

1111 **Immunoblotting**

1112 Mouse and human MEC were collected post-treatment and lysed in
 1113 RIPA buffer. Protein content was measured using the Bio-Rad Protein Assay
 1114 (Bio-Rad). Samples were resuspended in 4X Bolt LDS Sample Buffer (Life
 1115 Technologies) and incubated at 70°C for 5 min before loading on precast
 1116 BOLT 4-12% Bis-Tris Plus gels (Life Technologies). Immunoblotting was per-
 1117 formed using a standard protocol and primary Abs recognizing the following
 1118 proteins: Aryl hydrocarbon Receptor (BML-SA210-0025, Enzo Life Sciences),
 1119 vinculin (SPM227, Abcam), amphiregulin (16036-1-IP, Proteintech), total EGF-
 1120 receptor (#4267, Cell Signaling), phospho-EGF receptor (Tyr1068) (#2234, Cell
 1121 Signaling), alpha-tubulin (T5168, Sigma) and actin (A2066, Sigma-Aldrich).
 1122 Primary Abs were visualized using anti-mouse and anti-rabbit ECL HRP-
 1123 conjugated secondary Abs (Amersham). Membranes were developed for
 1124 chemiluminescent detection and images were acquired with GelCapture
 1125 Software using MicroChem 2.0/4.2 (FroggaBio).

1126 **ELISA and cytokine profiling**

1127 Detection of mouse and human amphiregulin in culture supernatants of
 1128 mouse and human MEC and human breast cancer cell lines was performed
 1129 using the Mouse and Human Amphiregulin DuoSet ELISA Kit (R&D) according
 1130 to manufacturer's protocol. Absorbance was determined at 450nm on a
 1131 FlexStation 3 plate reader (Molecular Devices). Cytokine profiling was con-
 1132 ducted using the Cytokine Array-Mouse Cytokine Antibody Array kit (Abcam)
 1133 according to manufacturer's instructions. Membranes were developed for
 1134 chemiluminescent detection and images were acquired with GelCapture
 1135 Software using MicroChem 2.0/4.2 (FroggaBio).

1136 **RT-PCR**

1137 RNA was isolated using the Nucleospin RNA Plus kit (Macherey-Nagel)
 1138 and reverse-transcribed using the iScript cDNA synthesis kit (Bio-Rad) accord-
 1139 ing to manufacturers' instructions. Quantitative RT-PCR was performed using
 1140 SYBR Green primers (Applied Biosystems). Mouse ribosomal protein S9 (rps9)
 1141 and human ribosomal protein S18 (rps18) were used as housekeeping genes
 1142 to determine relative mRNA expression. All primer sequences are described
 1143 in SI Appendix, Table S1.

1144 **RNA sequencing**

1145 Total RNA was isolated from MEC and KBP mammary tumors using
 1146 the Nucleospin RNA Plus kit (Macherey-Nagel). Zug of RNA were assessed
 1147 for quality control using the Agilent Bioanalyzer prior to library construc-
 1148 tion. RNA deep sequencing was performed with the Illumina HiSeq 2000
 1149 sequencing system at Princess Margaret Genomic Centre (Toronto, Canada).
 1150 Processed sequence data were obtained as .fastq files along with FASTQC
 1151 data. The regularized log-normalized (rlog) expression values were plotted
 1152 by transforming the count data to the log2 scale according to the method
 1153 previously described by Love et al.(55).

- 1154 1. Cairns RA, Harris IS, & Mak TW (2011) Regulation of cancer cell metabolism. *Nat Rev*
- 1155 *Cancer* 11(2):85-95.
- 1156 2. Gorini C, Harris IS, & Mak TW (2013) Modulation of oxidative stress as an anticancer
- 1157 strategy. *Nat Rev Drug Discov* 12(12):931-947.
- 1158 3. Lyssiotis CA & Kimmelman AC (2017) Metabolic Interactions in the Tumor Microenviron-
- 1159 ment. *Trends Cell Biol* 27(11):863-875.
- 1160 4. Munn DH & Mellor AL (2013) Indoleamine 2,3 dioxygenase and metabolic control of
- 1161 immune responses. *Trends in immunology* 34(3):137-143.
- 1162 5. Chang CH, et al. (2013) Posttranscriptional control of T cell effector function by aerobic
- 1163 glycolysis. *Cell* 153(6):1239-1251.
- 1164 6. Chang CH, et al. (2015) Metabolic Competition in the Tumor Microenvironment Is a Driver
- 1165 of Cancer Progression. *Cell* 162(6):1229-1241.
- 1166 7. Takahashi N, et al. (2018) Cancer Cells Co-opt the Neuronal Redox-Sensing Channel TRPA1

Chromatin immunoprecipitation

ChIP was performed in COMMA-1D cells as previously described (56)
 with the following modifications: AhR protein (4 μ g; Enzo Life Sciences) was
 prebound to Protein A and G Dynabeads (Life Technologies) for 6 hr. DNA
 fragments were purified with the MinElute PCR purification kit (Qiagen) and
 processed for quantitative PCR analysis according to the manufacturer's pro-
 tocol. Fold enrichment was calculated over input. The statistical significance
 of differences in enrichment was calculated using the unpaired Student t-
 test. A complete list of PCR primers appears in SI Appendix, Table S2.

ROS measurement

To measure intracellular ROS, cells were incubated with 300 nM CM-
 H₂DCFDA (DCF-DA, C6827, Invitrogen) for 10 min at 37°C. DCF-DA fluores-
 cence was analyzed by flow cytometry using a FACS Canto instrument (BD
 Biosciences) and FlowJo software.

Immunocytochemistry (ICC)

COMMA-1D were seeded onto glass coverslips in 12 well plates in
 triplicates (1 \times 10⁵/well). Cells were treated with BSO at 200 μ M for 1h. Cells
 were fixed with paraformaldehyde (2% PAF) at room temperature for 10min
 and then washed with PBS1X twice. Cells were incubated with Blocking
 buffer containing 10% FBS and 0.05% Triton in PBS1X at room temperature
 for 1h. Primary antibody (Aryl hydrocarbon Receptor (BML-SA210-0025, Enzo
 Life Sciences) was diluted at 1/100 in Blocking buffer and applied at room
 temperature for 1h. Cells were washed with 2% FBS Blocking buffer three
 times prior incubation with secondary antibody (goat anti-rabbit Alexa Fluor
 568, ThermoFisher Scientific) at 1/1000 at room temperature for 1h. Cells
 were washed with 2% FBS Blocking buffer three times and then stained
 with DAPI (0.5 μ g/ml in PBS1X) at room temperature for 5min. Coverslips
 were rinsed in water and mount with VectaShield (50ul/coverslip, Vector
 Laboratories). Images were acquired with a fluorescence microscope (Zeiss
 AxioImager M1 equipped with Hamamatsu ORCA Flash4 camera) using Zeiss
 Zen software and processed with Adobe Photoshop CS5. Data were reported
 as percentage of cells with AhR positive nuclear staining per total number of
 cells (n=100).

Statistical analyses of mouse and human cell line data

Data were reported in bar graphs as the mean or median \pm standard
 error of the mean (SEM), with p-values calculated using Student's t-test
 (* \leq 0.05, ** \leq 0.01, *** \leq 0.001). The mean was calculated based on a minimum
 of n=3 replicates in each experiment, and each experiment was performed
 at least 3 times. Data were analyzed either by Microsoft Excel or GraphPad
 Prism 7.

AUTHOR CONTRIBUTIONS

S.P.K and C.B. designed and performed experiments, analyzed data and
 co-wrote the paper; C.R. performed experiments and analyzed data; A.W.,
 J.H. and M.F. performed and supervised in vivo mouse studies; C.G., W.J., B.S.
 and L.J. generated and characterized MDA-MB-468 AhR wild-type and knock-
 out lines; L.P., K.T., and P.R. performed bioinformatic analysis; L.C., D.S., C.H.,
 C.L., C.G., T.B. and A.P. performed and analyzed immunohistochemical stain-
 ing of human breast cancer tissues; S.P.B., G.D. and P.T. provided technical
 support; M.S. and Y.Y. gave conceptual advice on EGFR signaling analysis;
 J.S.S. and D.W.C. provided technical and conceptual assistance for the drug
 sensitivity screen; S.P., J.W.P. and T.W.M gave conceptual advice; M.A.P. gave
 conceptual advice and supervised bioinformatic and immunohistochemical
 analyses; P.C. gave conceptual advice and contributed to the design and
 execution of immune system analysis; C.G. conceived the project, designed
 and performed experiments, analyzed data and co-wrote the paper.

ACKNOWLEDGEMENTS

This study was supported by Susan G. Komen Career Catalyst Research
 Grant 410005437 (C.G.), CIHR MOP-86707 (T.W.M.), Foundation CIHR grant
 FDN 143268 (T.W.M.), Spanish Ministry of Health ISCIII grant PI15/00854
 and PI18/01029 (M.A.P.), Spanish Ministry of Science and Innovation "Fondo
 Europeo de Desarrollo Regional (FEDER) (M.A.P.), Generalitat de Catalunya
 SGR-2017-449 and CERCA Program (M.A.P.), Asociación Española Contra el
 Cáncer (Hereditary Cancer grant; C.L. and M.A.P.) and University of Turin-
 Compagnia di San Paolo (PANTHER for P.C.). We thank Mary Saunders for
 scientific editing of the manuscript; Rob Cairns for helpful discussions; Thales
 Papagiannakopoulos for assistance with CRISPR/Cas9 gene editing experi-
 ments; and Arianna Sabo, Bruno Amati and Mathieu Lupien for assistance
 in performing ChIP assays.

- to Promote Oxidative-Stress Tolerance. *Cancer Cell* 33(6):985-1003 e1007.
8. Port J, et al. (2018) Colorectal Tumors Require NIAK1 for Protection from Oxidative Stress. *Cancer Discov* 8(5):632-647.
9. Gross MI, et al. (2014) Antitumor activity of the glutaminase inhibitor CB-839 in triple-negative breast cancer. *Mol Cancer Ther* 13(4):890-901.
10. Long JP, Li XN, & Zhang F (2016) Targeting metabolism in breast cancer: How far we can go? *World J Clin Oncol* 7(1):122-130.
11. Timmerman LA, et al. (2013) Glutamine sensitivity analysis identifies the xCT antiporter as a common triple-negative breast tumor therapeutic target. *Cancer Cell* 24(4):450-465.
12. Gorini C, et al. (2013) BRCA1 interacts with Nrf2 to regulate antioxidant signaling and cell survival. *J Exp Med* 210(8):1529-1544.
13. Maddocks OD & Vousden KH (2011) Metabolic regulation by p53. *J Mol Med (Berl)* 89(3):237-245.

1225
1226
1227
1228
1229
1230
1231
1232
1233
1234
1235
1236
1237
1238
1239
1240
1241
1242
1243
1244
1245
1246
1247
1248
1249
1250
1251
1252
1253
1254
1255
1256
1257
1258
1259
1260
1261
1262
1263
1264
1265
1266
1267
1268
1269
1270
1271
1272
1273
1274
1275
1276
1277
1278
1279
1280
1281
1282
1283
1284
1285
1286
1287
1288
1289
1290
1291
1292

14. Murray IA, Patterson AD, & Perdew GH (2014) Aryl hydrocarbon receptor ligands in cancer: friend and foe. *Nat Rev Cancer* 14(12):801-814.

15. Denison MS & Nagy SR (2003) Activation of the aryl hydrocarbon receptor by structurally diverse exogenous and endogenous chemicals. *Annu Rev Pharmacol Toxicol* 43:309-334.

16. Hayes JD, Dinkova-Kostova AT, & McMahon M (2009) Cross-talk between transcription factors AhR and Nrf2: lessons for cancer chemoprevention from dioxin. *Toxicol Sci* 111(2):199-201.

17. Griffith OW & Meister A (1979) Potent and specific inhibition of glutathione synthesis by buthionine sulfoximine (S-n-butyl homocysteine sulfoximine). *J Biol Chem* 254(16):7558-7560.

18. Luecke-Johansson S, *et al.* (2017) A Molecular Mechanism To Switch the Aryl Hydrocarbon Receptor from a Transcription Factor to an E3 Ubiquitin Ligase. *Mol Cell Biol* 37(13).

19. Yang X, *et al.* (2008) Constitutive regulation of CYP1B1 by the aryl hydrocarbon receptor (AhR) in pre-malignant and malignant mammary tissue. *J Cell Biochem* 104(2):402-417.

20. Walisser JA, Glover E, Pande K, Liss AL, & Bradfield CA (2005) Aryl hydrocarbon receptor-dependent liver development and hepatotoxicity are mediated by different cell types. *Proc Natl Acad Sci U S A* 102(49):17858-17863.

21. Chuang YY, *et al.* (2002) Gene expression after treatment with hydrogen peroxide, menadione, or t-butyl hydroperoxide in breast cancer cells. *Cancer Res* 62(21):6246-6254.

22. Sullivan LB & Chandel NS (2014) Mitochondrial reactive oxygen species and cancer. *Cancer Metab* 2:17.

23. Du B, Altorki NK, Kopelovich L, Subbaramaiah K, & Dannenberg AJ (2005) Tobacco smoke stimulates the transcription of amphiregulin in human oral epithelial cells: evidence of a cyclic AMP-responsive element binding protein-dependent mechanism. *Cancer Res* 65(13):5982-5988.

24. John K, Lahoti TS, Wagner K, Hughes JM, & Perdew GH (2014) The Ah receptor regulates growth factor expression in head and neck squamous cell carcinoma cell lines. *Mol Carcinog* 53(10):765-776.

25. Roskoski R, Jr. (2014) The ErbB/HER family of protein-tyrosine kinases and cancer. *Pharmacol Res* 79:34-74.

26. Bublit EM & Yarden Y (2007) The EGF receptor family: spearheading a merger of signaling and therapeutics. *Curr Opin Cell Biol* 19(2):124-134.

27. Kruspig B, *et al.* (2018) The ERBB network facilitates KRAS-driven lung tumorigenesis. *Sci Transl Med* 10(446).

28. Sternlicht MD & Sunnarborg SW (2008) The ADAM17-amphiregulin-EGFR axis in mammary development and cancer. *J Mammary Gland Biol Neoplasia* 13(2):181-194.

29. Liu X, *et al.* (2007) Somatic loss of BRCA1 and p53 in mice induces mammary tumors with features of human BRCA1-mutated basal-like breast cancer. *Proc Natl Acad Sci U S A* 104(29):12111-12116.

30. Gorrini C, *et al.* (2014) Estrogen controls the survival of BRCA1-deficient cells via a PI3K-NRF2-regulated pathway. *Proc Natl Acad Sci U S A* 111(12):4472-4477.

31. Julliard W, Fechner JH, & Mezrich JD (2014) The aryl hydrocarbon receptor meets immunology: friend or foe? A little of both. *Front Immunol* 5:458.

32. Zaiss DMW, Gause WC, Osborne LC, & Artis D (2015) Emerging functions of amphiregulin in orchestrating immunity, inflammation, and tissue repair. *Immunity* 42(2):216-226.

33. Opitz CA, *et al.* (2011) An endogenous tumour-promoting ligand of the human aryl hydrocarbon receptor. *Nature* 478(7368):197-203.

34. Platten M, von Knebel Doeberitz N, Oezen I, Wick W, & Ochs K (2014) Cancer Immunotherapy by Targeting IDO1/TDO and Their Downstream Effectors. *Front Immunol* 5:673.

35. Zaiss DM, *et al.* (2013) Amphiregulin enhances regulatory T cell-suppressive function via the epidermal growth factor receptor. *Immunity* 38(2):275-284.

36. Noy R & Pollard JW (2014) Tumor-associated macrophages: from mechanisms to therapy. *Immunity* 41(1):49-61.

37. Jakubzick C, *et al.* (2013) Minimal differentiation of classical monocytes as they survey steady-state tissues and transport antigen to lymph nodes. *Immunity* 39(3):599-610.

38. Mantovani A, *et al.* (2004) The chemokine system in diverse forms of macrophage activation and polarization. *Trends Immunol* 25(12):677-686.

39. Lanaya H, *et al.* (2014) EGFR has a tumour-promoting role in liver macrophages during hepatocellular carcinoma formation. *Nat Cell Biol* 16(10):972-977.

40. Srivatsa S, *et al.* (2017) EGFR in Tumor-Associated Myeloid Cells Promotes Development of Colorectal Cancer in Mice and Associates With Outcomes of Patients. *Gastroenterology* 153(1):178-190 e110.

41. Pollard JW (2004) Tumour-educated macrophages promote tumour progression and metastasis. *Nat Rev Cancer* 4(1):71-78.

42. Gouon-Evans V, Rothenberg ME, & Pollard JW (2000) Postnatal mammary gland development requires macrophages and eosinophils. *Development* 127(11):2269-2282.

43. Franklin RA, *et al.* (2014) The cellular and molecular origin of tumor-associated macrophages. *Science* 344(6186):921-925.

44. Youn JI, Nagaraj S, Collazo M, & Gabrilovich DI (2008) Subsets of myeloid-derived suppressor cells in tumor-bearing mice. *J Immunol* 181(8):5791-5802.

45. Mantovani A, Bonecchi R, & Locati M (2006) Tuning inflammation and immunity by chemokine sequestration: decoys and more. *Nat Rev Immunol* 6(12):907-918.

46. Martinez FO, Helming L, & Gordon S (2009) Alternative activation of macrophages: an immunologic functional perspective. *Annu Rev Immunol* 27:451-483.

47. Ali R & Wendt MK (2017) The paradoxical functions of EGFR during breast cancer progression. *Signal Transduct Target Ther* 2.

48. Kappler CS, *et al.* (2015) Oncogenic signaling in amphiregulin and EGFR-expressing PTEN-null human breast cancer. *Mol Oncol* 9(2):527-543.

49. Hobor S, *et al.* (2014) TGFalpha and amphiregulin paracrine network promotes resistance to EGFR blockade in colorectal cancer cells. *Clin Cancer Res* 20(24):6429-6438.

50. Busser B, *et al.* (2010) Amphiregulin promotes BAX inhibition and resistance to gefitinib in non-small-cell lung cancers. *Molecular therapy : the journal of the American Society of Gene Therapy* 18(3):528-535.

51. Ishikawa N, *et al.* (2005) Increases of amphiregulin and transforming growth factor-alpha in serum as predictors of poor response to gefitinib among patients with advanced non-small cell lung cancers. *Cancer Res* 65(20):9176-9184.

52. Zhao B, Degroot DE, Hayashi A, He G, & Denison MS (2010) CH223191 is a ligand-selective antagonist of the Ah (Dioxin) receptor. *Toxicol Sci* 117(2):393-403.

53. Stockinger B, Di Meglio P, Gialitakis M, & Duarte JH (2014) The aryl hydrocarbon receptor: multitasking in the immune system. *Annu Rev Immunol* 32:403-432.

54. Sousa S, *et al.* (2015) Human breast cancer cells educate macrophages toward the M2 activation status. *Breast Cancer Res* 17:101.

55. Love MI, Huber W, & Anders S (2014) Moderated estimation of fold change and dispersion for RNA-seq data with DESeq2. *Genome Biol* 15(12):550.

56. Bailey SD, *et al.* (2016) Noncoding somatic and inherited single-nucleotide variants converge to promote ESR1 expression in breast cancer. *Nat Genet* 48(10):1260-1266.

1293
1294
1295
1296
1297
1298
1299
1300
1301
1302
1303
1304
1305
1306
1307
1308
1309
1310
1311
1312
1313
1314
1315
1316
1317
1318
1319
1320
1321
1322
1323
1324
1325
1326
1327
1328
1329
1330
1331
1332
1333
1334
1335
1336
1337
1338
1339
1340
1341
1342
1343
1344
1345
1346
1347
1348
1349
1350
1351
1352
1353
1354
1355
1356
1357
1358
1359
1360

SI Appendix Material and Methods (Analysis of human samples)

Immunohistochemistry (IHC)

Women carrying BRCA1/2 mutations were recruited by the Genetic Counseling Unit of the Catalan Institute of Oncology, L'Hospitalet (Barcelona). The IDIBELL's Ethics Committee approved the study protocol and written informed consent was obtained from all participants. Control breast tissue samples were acquired from anonymous premenopausal women undergoing reduction mastectomy at the University Hospital of Bellvitge, IDIBELL. IHC was performed as previously described(12). Tissue samples were incubated overnight at 4°C with anti-amphiregulin primary Ab (16036-1 AP, Proteintech) at a dilution of 1:100. Specimens were viewed with a brightfield microscope (Leica DM2500 equipped with Micropublisher 3.3-QI imaging camera) using Q-Capture Pro Software and processed with Adobe Photoshop CS5.

For identification of human CD163-positive macrophages in human breast cancers, IHC was performed with CD163 primary antibody (MCA1853, Bio-Rad) as previously described(57). AREG positive regions were identified by pre-segmenting the images at 10x magnification using multiresolution segmentation in Definiens DeveloperXD (scale = 800, shape coefficient = 0.4, compactness coefficient = 0.1) and classified based on the object's mean intensity, the number of standard deviations from the image mean in AREG stain channel, its relative brightness compared to neighbour objects, and with shape morphometrics. AREG positive regions were grown by 20 pixels (~26µm) up to 100 pixels in order to fill gaps between very close AREG positive objects, to include immediately adjacent stroma, and to combine small regions of AREG positive epithelium that, in a 3D setting, would have come from the same structure. AREG negative regions were identified as any regions which was not AREG positive or one of the pixel-distance bins. Any misclassified regions were manually corrected. Images were captured with Olympus IX81 fluorescence microscope and processed with ZEN imaging software, CZI. Data were analyzed by GraphPad Prism 7.

For IHC staining of mouse KBP tumors, tissue specimens were incubated with primary Abs to detect amphiregulin (16036-1 AP, Proteintech), F4/80 (MCA497GAR, Bio-Rad), and CD31(AB28364, Abcam). For amphiregulin, we applied the same conditions as for human breast cancer specimen as described above. For F4/80 staining, antigen retrieval

for performed with Proteinase K (PK) treatment at 37°C for 10 min. The primary Ab was prepared in 5% rabbit serum with 0,2% Triton X-100 at a dilution of 1:200 overnight at 4°C. Secondary Ab (Vector labs BA-4001) was incubated for 30 min at a dilution of 1:400. For IHC staining of CD31 positive cells tissue samples were incubated in 10mM Na Citrate (pH6) solution. The primary Ab was diluted at 1:50 dilution in DAKO Protein block and incubated for 45 minutes at room temperature. Secondary Ab (Jackson Labs) was diluted 1:400 and incubated for 45 minutes. In both cases, slides were digitized using a Nanozoomer2.0 HT-Hamamatsu (Olympus). An image analysis protocol (APP) was developed using Visiopharm software (Visiopharm, Denmark) to identify the area of IHC staining positive for F480 and CD31. A ratio of positive expression to region of interest was then calculated for each test group. In both human breast cancer and mouse tumor specimen, DAPI was used as nuclear staining.

Analysis of human breast cancer datasets

The results published here are partly based upon data generated by TCGA managed by the National Cancer Institute (NCI) and the National Human Genome Research Institute (NHGRI). Information about TCGA can be found at <http://cancergenome.nih.gov>. HR-deficient BC cohort was defined by using TCGA breast cancer RNAseq data and somatic mutations after being obtained following approval by the Data Access Committee (project #11689). Mutational signatures were defined using the R mut Signatures package(58). The GSEA tool was run with default values for all parameters.

Gene expression differences stratified according to BRCA1 mRNA level were analyzed using preprocessed and normalized RNA-seq and microarray expression TCGA data (downloaded from the GDC data portal on 2016-04-22). For each gene, a logistic regression analysis was implemented to assess its association with the expression level of BRCA1, categorized in tertiles. Unadjusted and adjusted (with covariates of ERBB2, ESR1, and PGR expression) models were used, which provided similar estimations. Gene expression correlations were computed using Pearson's correlation coefficient, and p-values indicated the probability of independence. Data were normalized to log2 standard TCGA normalization. Rosetta microarray-derived gene expression data along with BRCA1 mutation status from the Van't Veer cohort were downloaded from <http://www.rii.com/publications/default.htm>(59). Because the expression profiles obtained

were log-ratio data, no further normalization was performed. Comparison of AhR, CYP1A1, and CYP1A2 expression levels in BRCA1-mutated versus wild-type breast tumors was performed using a two-tailed Mann-Whitney U test and GraphPad Prism Software.

PAM50 calls annotated in clinical data were used to identify primary breast tumors of the basal subtype (n=141) which were segregated into quartiles based on *AREG* mRNA levels. Candidate gene expression levels were then compared in tumors in the top and bottom quartiles. Expression profiles were subjected to single sample gene set enrichment analysis (ssGSEA) using the Broad's GenePattern tool to derive individual tumor enrichment scores for a panel of MSigDB gene-sets corresponding to the cellular response to oxidative stress (<http://software.broadinstitute.org/cancer/software/genepattern/>)(60, 61). The "Chuang_oxidative_stress_response" gene set (ROS up-regulated genes only) displayed the greatest variance in ssGSEA enrichment scores across tumors and was chosen for subsequent analysis. Tumors were classified into quartiles based on their ssGSEA scores for this gene-set. AhR, CYP1B1, AREG, CCL5, CXCL1 and CXCL2 expression levels were then compared between tumors in the top and bottom quartiles, representing those with high and low responses to oxidative stress, respectively. All two-group statistical comparisons of gene expression levels were performed using a two-tailed Mann-Whitney U test and GraphPad Prism Software.

The immune cell content in tumors was inferred using the Microenvironment Cell Populations-counter method (62). These analyses and PCC computations were performed in R software.

The AHR and AHR-ARNT target gene sets were obtained from the TRANSFAC database(63). The expression signature scores were computed using the ssGSEA algorithm with standard parameters and using all genes included in each set. The Pearson's correlation coefficients and p-values were computed in R.

Cancer Cell Line Encyclopedia was used to investigate the expression of AhR in human breast cancer cell lines(64, 65). The cell lines were grouped into basal-like and non-basal-like based on the method previously described(66).

SI Appendix Figure Legends

Figure S1. AhR expression and activation in NRF2-deleted cells and BC with high ROS levels. (A) AhR mRNA levels in human MCF10A cells left untreated (Ctr) or treated with 200 μ M BSO for 24h. (B) Representative images of immunofluorescence assay in COMMA-1D cells treated with 200 μ M BSO for 1h or left untreated (Ctr). Blue=nuclear staining with Dapi, Magenta=AhR staining. The cells contained in dashed rectangles are reported in Figure 1D as example of scoring criteria of low/undetectable or positive AhR nuclear signal. Scale bar=20 μ m. (C) Expression levels of Ahr exon2 in mouse MEC that were isolated from Ahr^{ff} mice, infected with cre-expressing (+cre) or empty vector (-cre) adenoviruses and then left untreated (Ctr) or treated with 50 μ M BSO for 24hr before analysis. (D) Nrf2 mRNA levels of mouse MEC isolated from Nrf2^{-/-} or Nrf2^{+/+} mice. (E) AhR mRNA levels of mouse MEC as in (D). (F, G) Hmox1 and Nqo1 mRNA levels of mouse MEC as in (D). (H) Nrf2 mRNA levels of COMMA-1D cells transfected with non-targeting (scramble, Scr) or mouse Nrf2 (siNrf2) siRNA oligos. Cells were analyzed at 48h post-transfection. (I) mRNA analysis of AhR-target Cyp1a1 in COMMA-1D cells that were transfected with single guide RNA against mouse AhR (sgAhR) and siRNA oligos specific for mouse Nrf2 (siNrf2) and then subjected to BSO (200 μ M) for 24h. Cells manipulated with empty vector (EV) and non-targeting (scramble, scr) siRNA were used as control. n=3/group. (J) mRNA levels of Ahr, CYP1A1 and CYP1A2 in the Van't Veer human BC dataset with tumors segregated by BRCA1 genotype: Wild-type, n=21; Mutated, n=18. (K) Inverse correlation between AhR or CYP1B1 expression with low or high BRCA1 mRNA levels in the TCGA human BC dataset.

Figure S2. Expression of AREG in normal and malignant mammary epithelial cells and analysis of Erbb receptors and ligands. (A) Immunoblot showing AREG protein in MCF10A cells that were left untreated (Ctr) or treated with 200 μ M BSO for 24hr or 48hr. (B) mRNA expression of mouse Erbb receptors as indicated in COMMA-1D cells. n=3. (C) mRNA expression of mouse Erbb ligands as indicated in COMMA-1D cells that were left untreated or subjected to 200 μ M BSO for 24h. n=3/group. (D) Quantification of AREG

expression in BRCA1 wild-type reduction mammoplasty from healthy women used as controls, prophylactic mastectomy specimen in women heterozygous for a BRCA1 mutation (BRCA1 mutant), and human BRCA1 mutant basal/TNBC breast tumours as shown in Figure 2J.

Figure S3. AhR-AREG axis has a pivotal role in BRCA1-associated tumorigenesis.

(A) mRNA levels of Nqo1 in KBP cells that were left untreated or treated with 200 μ M BSO for 24h. n=3/group. (B) Representative flow plots of DNA synthesis in KBP cells that were transfected with empty vector (EV), or vectors expressing sgAhr or sgAreg constructs, and examined at 24hr or 48hr after puromycin selection. (C) Representative images of EV-, sgAhr- or sgAreg- expressing KBP tumors (red arrows) in the mice on day 35 post-transplantation. (D) Growth curve of EV-, sgAhr- or sgAreg- expressing KBP cells by SRB colorimetric assay at different time points. (E) RNAseq data obtained from RNA deep sequencing of mouse MEC and KBP tumors (n=3/group). The lower and upper hinges correspond to the first and third quartiles (the 25th and 75th percentiles). The upper whisker extends from the hinge to the largest value no further than 1.5 * IQR from the hinge, and the lower whisker extends from the hinge to the smallest value at most 1.5 * IQR of the hinge (where IQR is the inter-quartile range, or distance between the first and third quartiles). (F) mRNA levels of Erbb ligands (Areg, Hbegf, Nrg1) in EV and sgAhr KBP tumors. n=3-5/group.

Figure S4. Analysis of tumour-infiltrating macrophages and bone marrow derived macrophages.

(A,B) Representative plots describing the gating strategy used to characterize macrophages in the mammary fat pad of virgin and nulliparous FVB female mice and KBP mammary tumors. (C) Histogram of phosphorylated EGFR (p-EGFR) signal in macrophages that were positive for CD11b and F4/80 surface markers (CD11b⁺F4/80⁺) in KBP tumors. Staining with isotype control was used to assess the specificity of the signal. (D) Left, representative image of the concentric regions “grown” from the area and at a distance spanning from 20pix to 100pix. Right, Quantification of CD163⁺ macrophages at different distances from an AREG-positive tumour area. (E) ELISA measurement of secreted VEGF-A protein in the medium of BMDM cultured alone, or after co-culture with KBP cells for 24hr (n=3/group). (F) Vegfa mRNA levels in KBP

cells alone (-) or after co-culturing with BMDM for 24 hr. (G) Egfr mRNA analysis in BMDM cultured alone, or after co-culture with KBP cells for 24hr (n=3/group).

Figure S5. Analysis of monocyte- and macrophage-related chemokines in BRCA1/p53-deleted mammary tumors. (A) Levels of the indicated chemokines in the culture medium of mouse MEC or KBP cells after 24hr culture (n=4/group). (B) Levels of the indicated chemokines in the culture medium of EV- or sgAhr-expressing KBP cells treated for 24hr with recombinant AREG (rAREG) at 50ng/ml. (C) Levels of CXCL1, CXCL2 and CCL5 mRNAs in TCGA BC grouped accordingly to low or high expression of BRCA1, AhR or AREG as indicated on the x-axis (n=1102).

Figure S6. Effect of AhR loss-of-function in human breast cancer and mouse mammary tumors. (A) mRNA levels of CYP1A1 in MDA-MB-468 cell line carrying a wild-type (AhR^{wt}) or deleted form of AhR (AhR^{ko}). Cells were left untreated (Ctr) or exposed to 500 μ M BSO for 24h. (B) Growth curve of MDA-MB-468 AhR^{wt} and AhR^{ko} cells for 4 days as measured by Tripin-blue exclusion assay. (C) Levels of secreted AREG in the media of the indicated cell lines that have been seeded and maintained in growth factor-rich media for 24h. (D,E) AREG levels in the culture medium of MDA-MB-468 and HCC1937 cell lines treated with increasing dose of the AhR inhibitor (AhRi), CH223191. (F) Immunoblot showing total EGFR, phosphorylated EGFR (P-EGFR) and AhR proteins in HCC1937 cells that were left untreated (Ctr) or treated with Erlotinib (E; 600nM) or AhRi (900nM) for 24 hr.

Figure S7. Sensitivity of breast cancer cell lines to AhR and EGFR inhibition. Synergy score plots as determined by analyzing data from 5-day SRB growth using the SynergyFinder web application. Red and green colors indicate the most synergistic or antagonist areas, respectively.

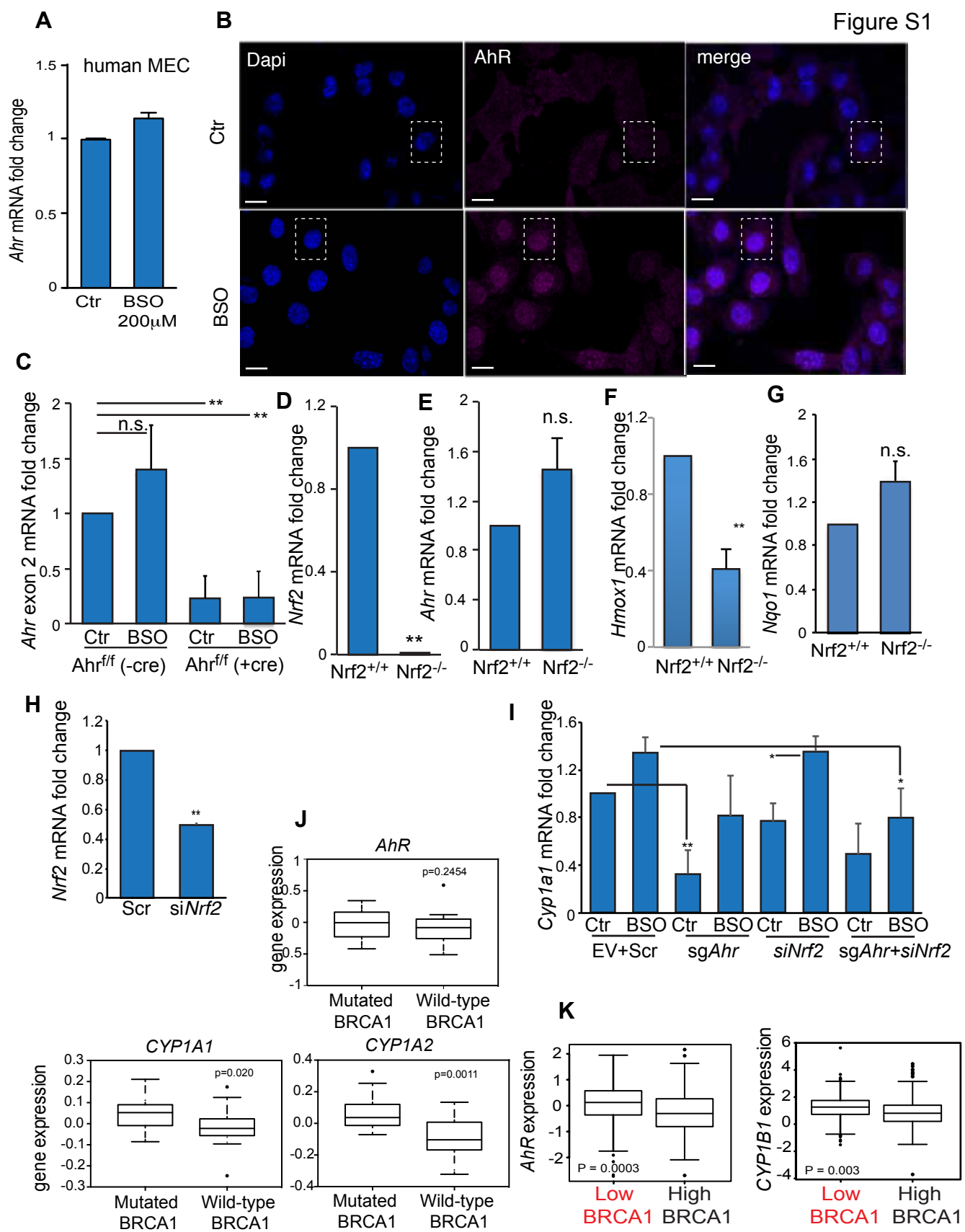


Figure S2

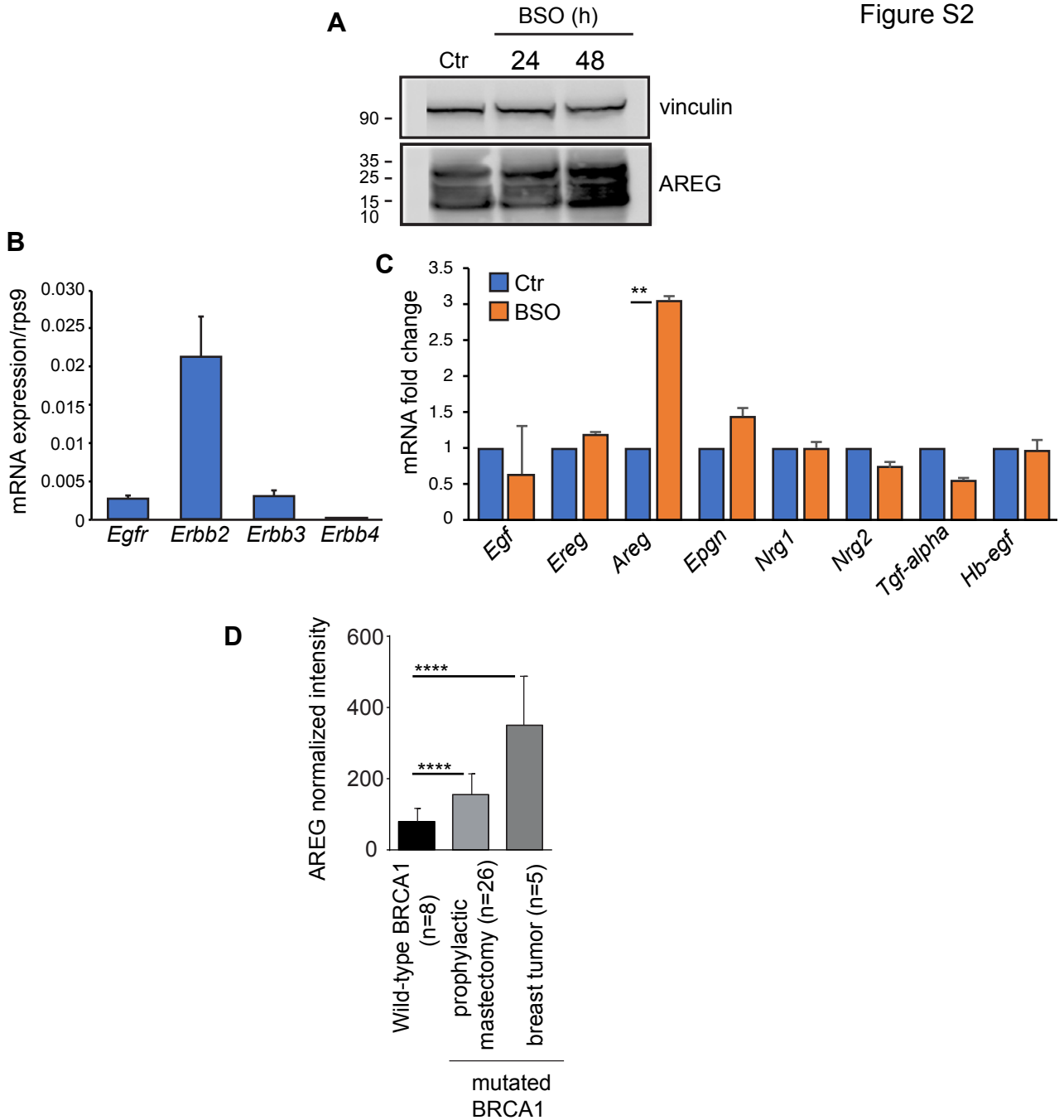


Figure S3

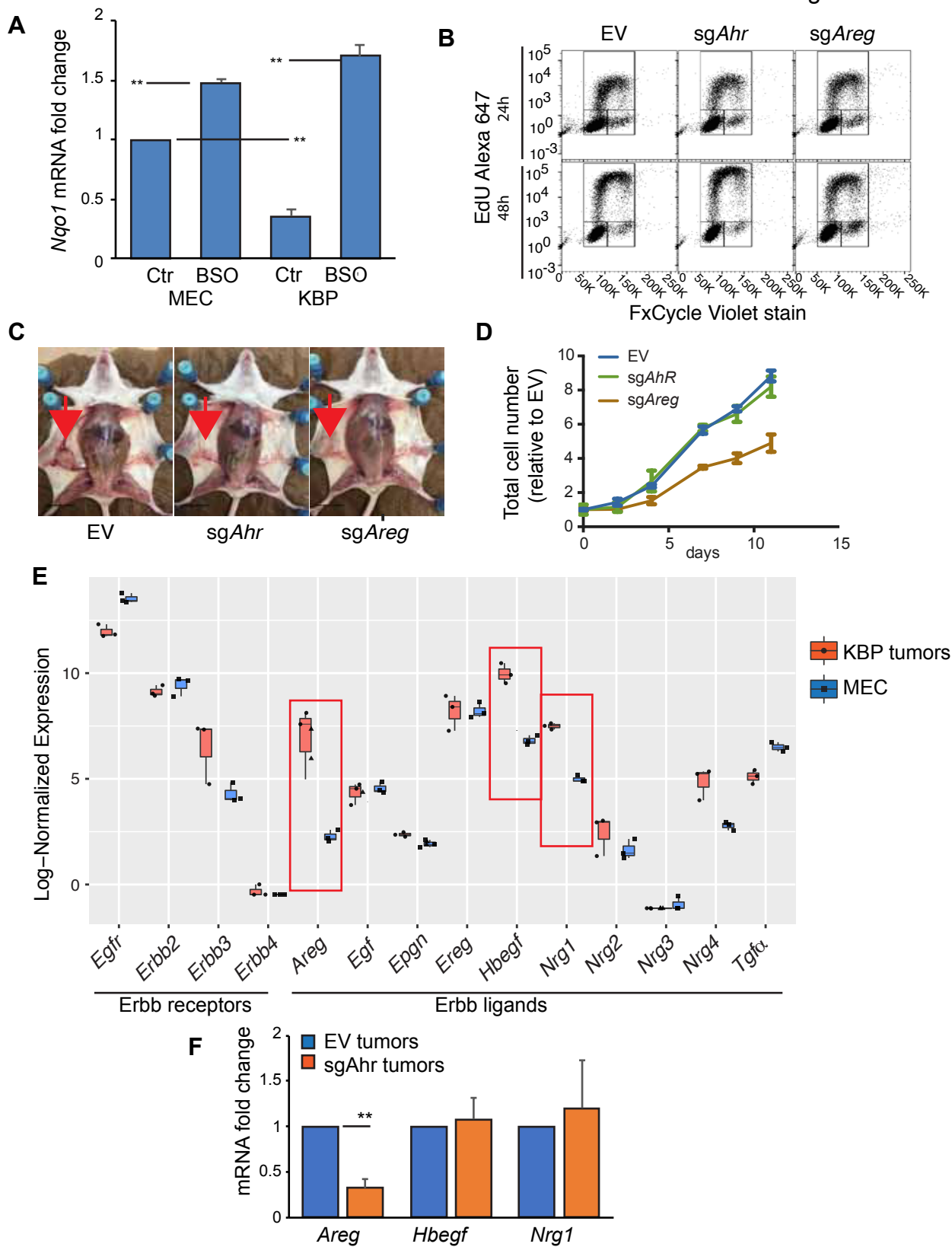


Figure S4

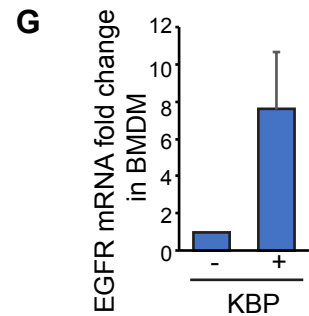
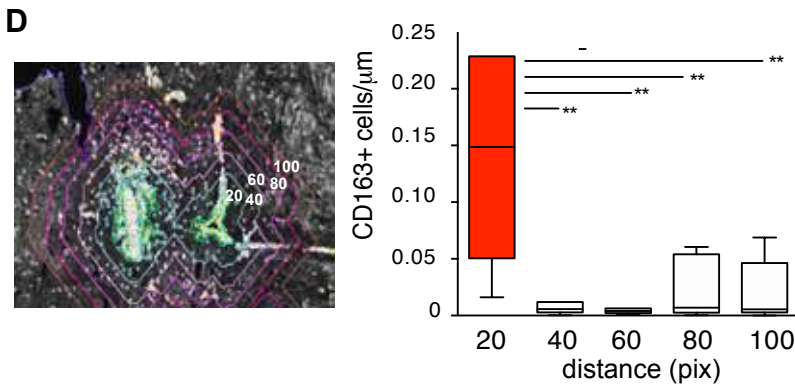
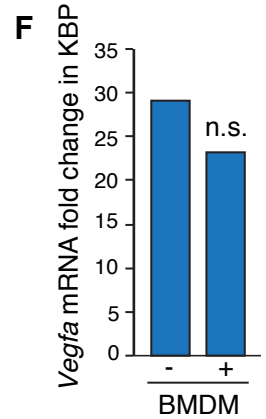
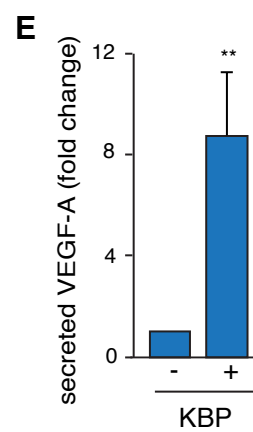
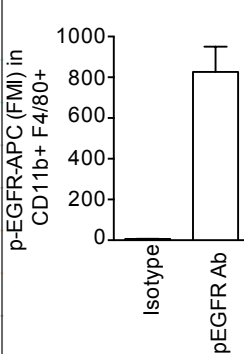
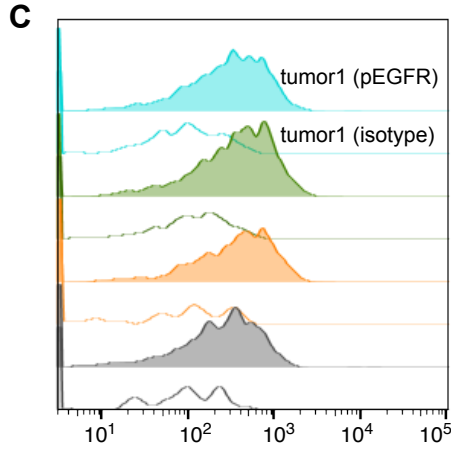
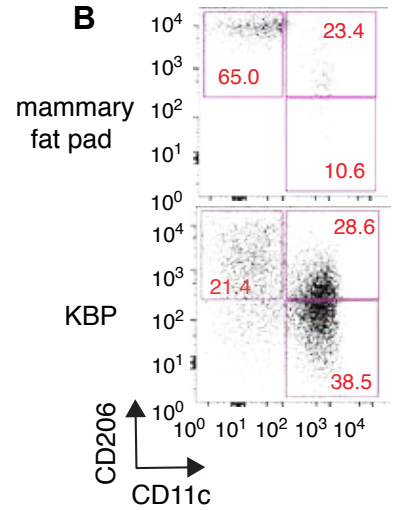
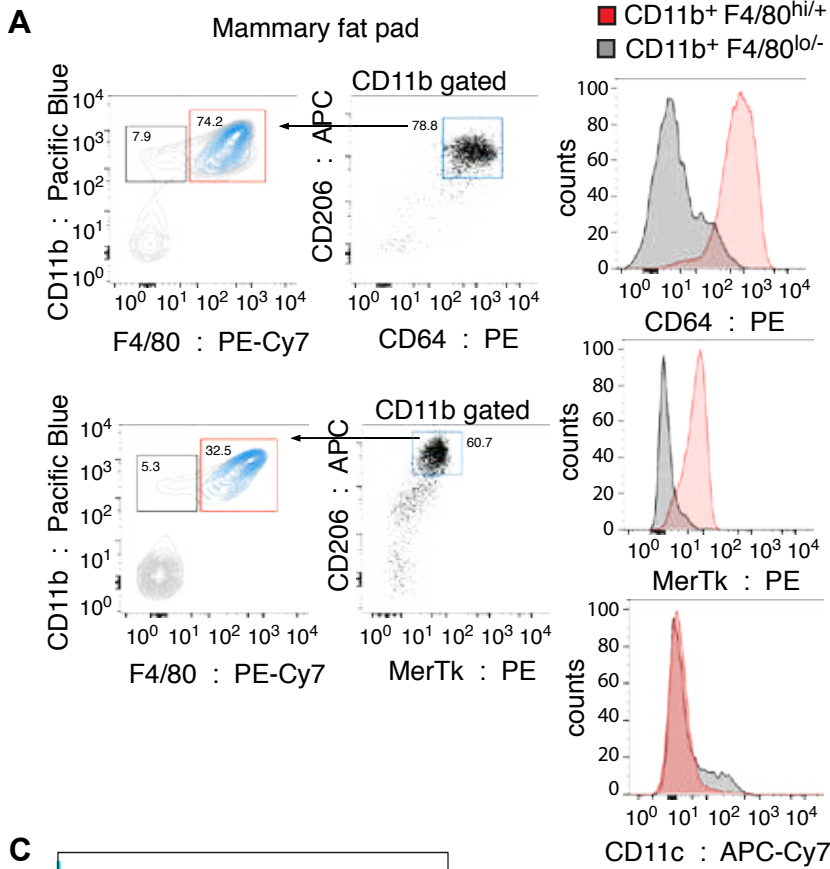


Figure S5

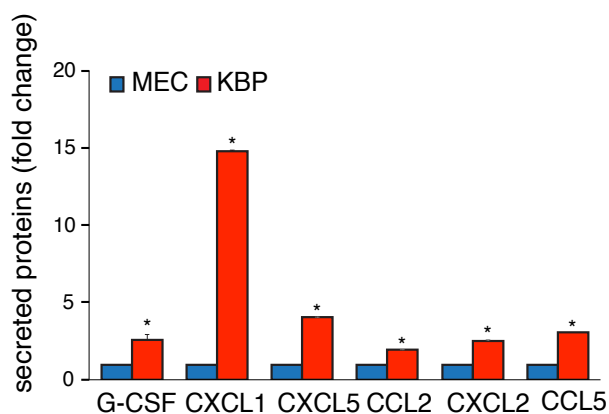
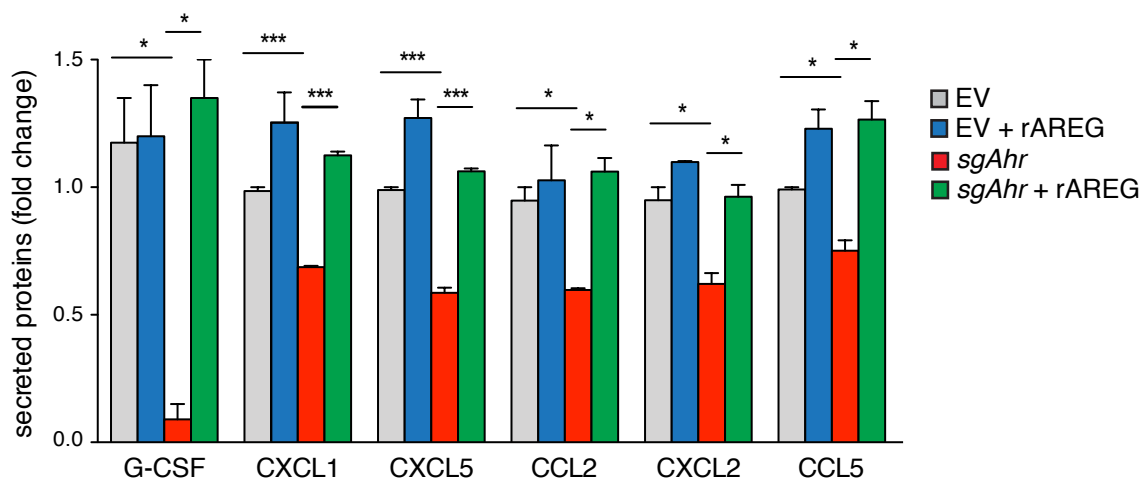
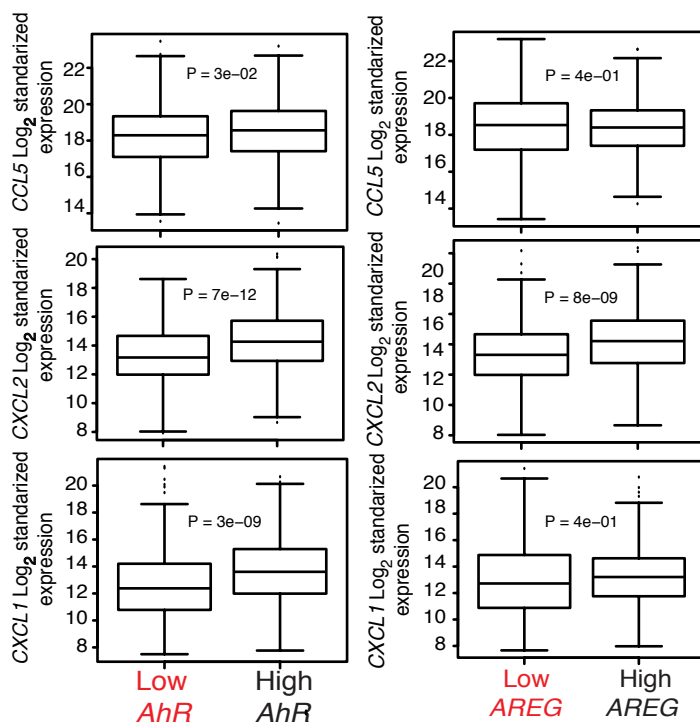
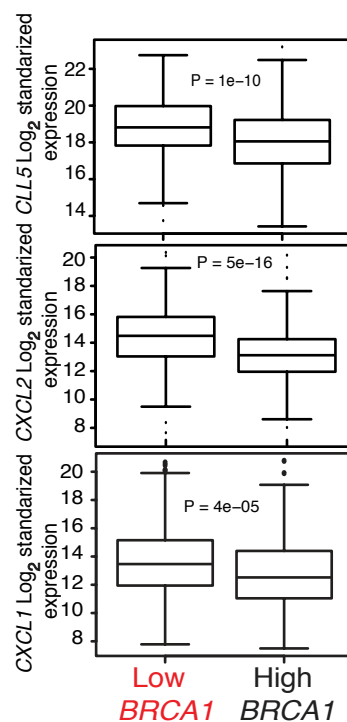
A**B****C****D**

Figure S6

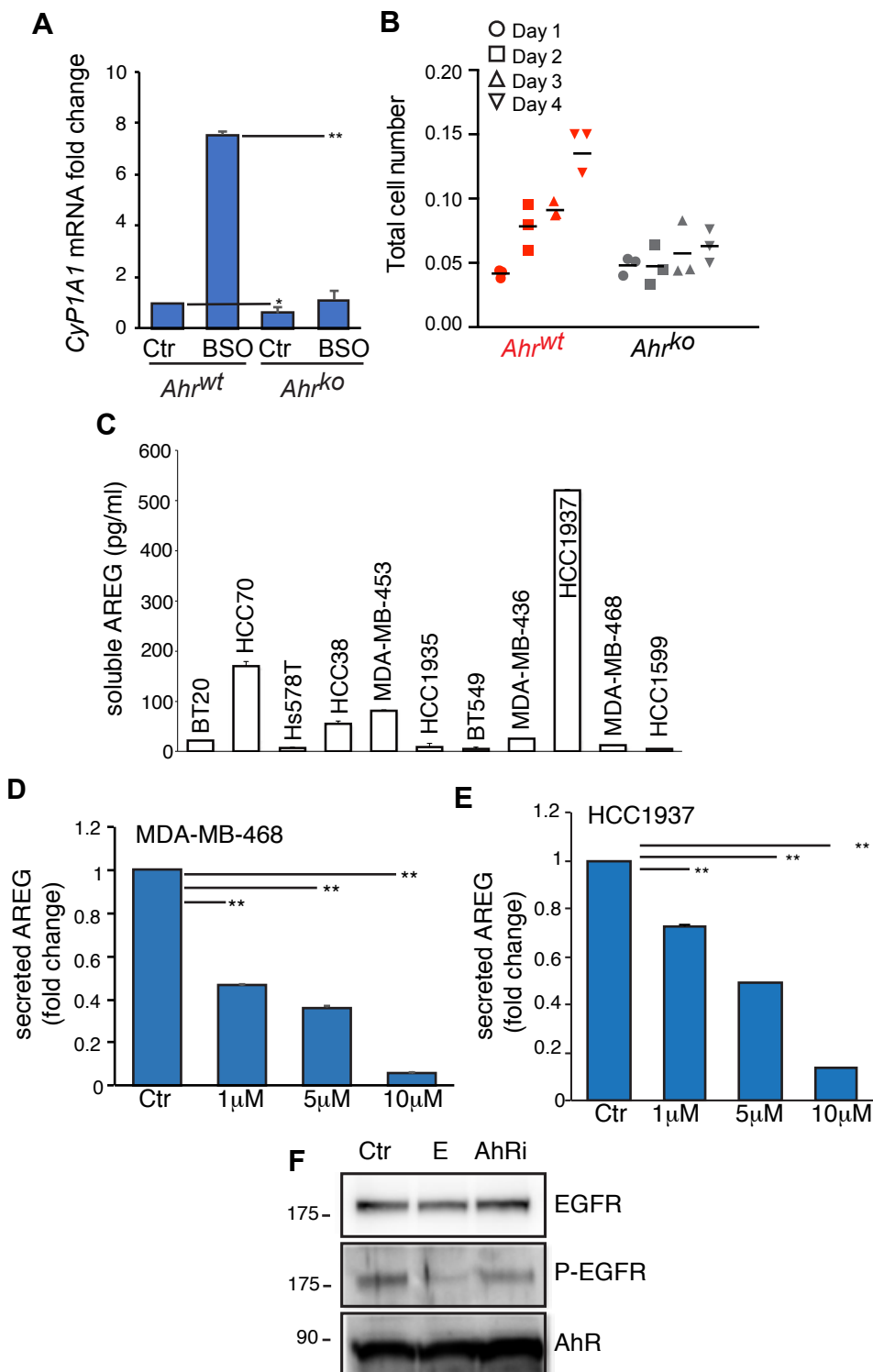
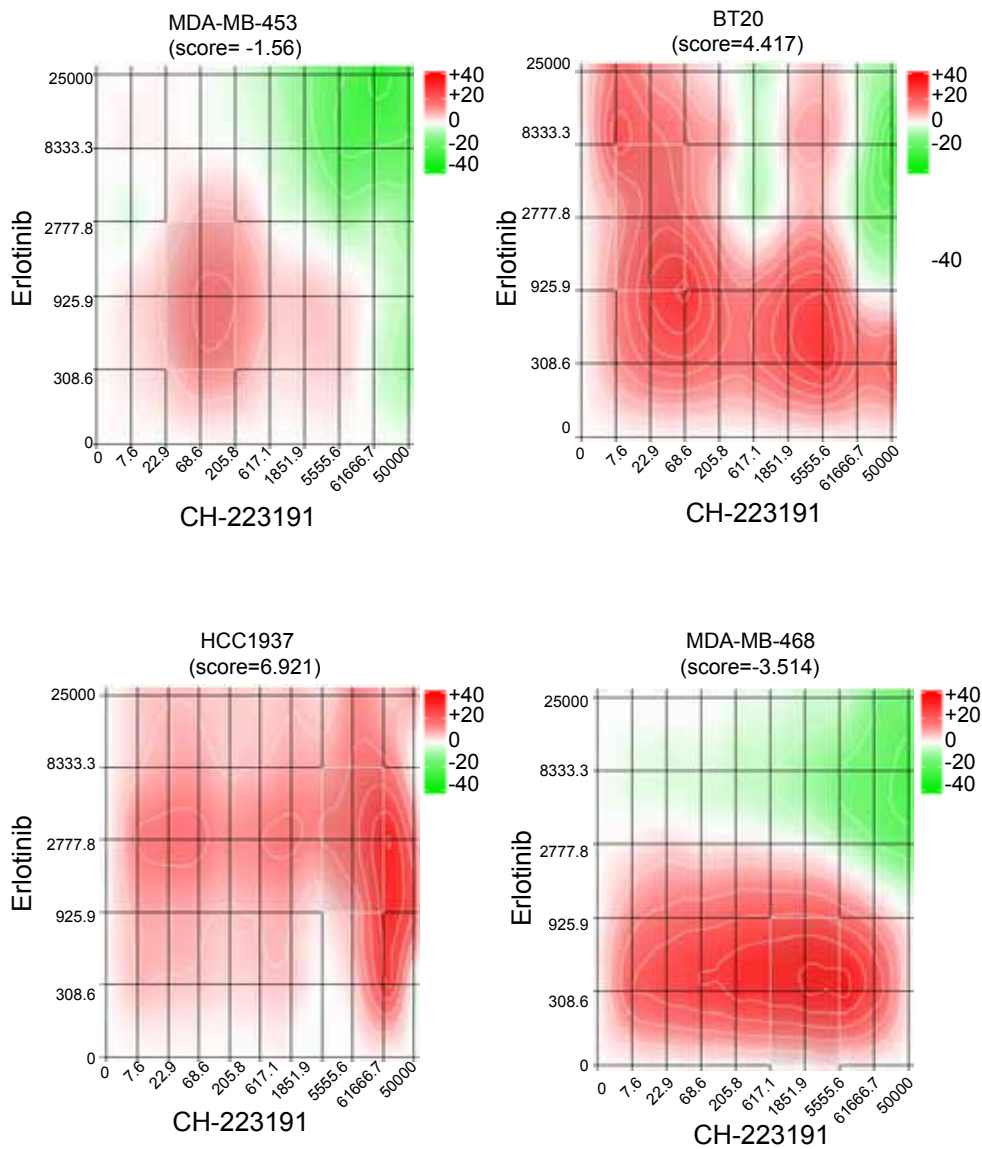


Figure S7



Supplementary Table 1: Primers used for qRT-PCR (m=mouse)

| Gene | Primer Sequence |
|--------------|--------------------------|
| mRps9 F | GCAAGATGAAGCTGGATTAC |
| mRps9 R | GGGATGTTCCACCACCTG |
| mNqo1 F | AGGATGGGAGGTACTCGAATC |
| mNqo1 R | AGGCGTCCTTCCTTATATGCTA |
| mHmox1 F | AAGCCGAGAATGCTGAGTTCA |
| mHmox1 R | GCCGTGTAGATAATGGTACAAGGA |
| mCypya1-F | CTCTTCCCTGGATGCCTTCAA |
| mCypya1-R | GGATGTGGCCCTTCTCAAATG |
| mAreg-F | GGTCTTAGGCTCAGGCCATT |
| mAreg-R | AGAGTTCACTGCCAGAAGGC |
| mAhr-F | CGGAGCGCTGCTTCCTCCAC |
| mAhr-R | GCTGCCCTTTGGCATCACAACC |
| mEgf-F | AGGATCCTGACCCCGAACTT |
| mEgf-R | ACAGCCGTGATTCTGAGTGG |
| mEpgn-F | TGGCTCTGGGGGTTCTGATA |
| mEpgn-R | TGTAGTCAGCTTCGGTGTTGT |
| mEreg-F | TGCTTTGTCTAGGTTCCCACC |
| mEreg-R | CGGGGATCGTCTTCCATCTG |
| mHbegf-F | TTTCTGGCCGCAGTGTTGTC |
| mHbegf-R | GTGGGTAGCAGCTGGTTTGT |
| mNrg1-F | GCAAAGAAGGCAGAGGCAAG |
| mNrg1-R | AATCTGGGAGGCAATGCTGG |
| mNrg2-F | CACTCTGTCATCCTGGTCGG |
| mNrg2-R | TCAGCCTTTTGCTTAGGATCTGG |
| mNrg3-F | CCTATCAAGCACACAGCCC |
| mNrg3-R | CCTGACCTCTATCCCTTGGC |
| mNrg4-F | TACGACGAGAGAAGTCCCAG |
| mNrg4-R | TAGCAGGGTGCAAGGTCAAC |
| mTgf_alpha_F | TAGCGCTGGGTATCCTGTTAG |
| mTgf_alpha_R | GAGTGTGGGAATCTGGGCAC |
| mEgfr-F | CACGCCAACTGTACCTATGGATGT |
| mEgfr-R | GGCCCAGAGGATTTGGAAGAA |
| mErbB2-F | GGCACTGTCTACAAGGGCAT |
| mErbB2-R | GAGGCGGGACACATATGGAG |
| mErbB3-F | CACCCAAGGGTGTAAGGGAC |
| mErbB3-R | CGCTCCAAGTAGCGTCTCAT |
| mErbB4-F | GGACGGGCCATTCCAATTTA |
| mErbB4-R | AAGGGCTCTACCAGCTCTGT |

SI Appendix Table 2: Primers used for ChIP-qPCR (m=mouse)

| | |
|---------------|-----------------------|
| mAreg_XRE_F | ttctccccgcgtaatcagg |
| mAreg_XRE_R | gccgggagggtactactccaa |
| mCyp1a1_XRE_F | caggcaacacagagaagtcg |
| mCyp1a1_XRE_R | aagcatcacccttgtagcc |